Geological Society, London, Special Publications

# Oligocene slow and Miocene–Quaternary rapid deformation and uplift of the Yumu Shan and North Qilian Shan: evidence from high-resolution magnetostratigraphy and tectonosedimentology

Xiaomin Fang, Dongliang Liu, Chunhui Song, Shuang Dai and Qingquan Meng

*Geological Society, London, Special Publications* 2013, v.373; p149-171.
doi: 10.1144/SP373.5



**Notes**

# Oligocene slow and Miocene–Quaternary rapid deformation and uplift of the Yumu Shan and North Qilian Shan: evidence from high-resolution magnetostratigraphy and tectonosedimentology

XIAOMIN FANG[1,2]*, DONGLIANG LIU[1,3], CHUNHUI SONG[2], SHUANG DAI[2] & QINGQUAN MENG[2]

[1]*Key Laboratory of Continental Collision and Plateau Uplift & Institute of Tibetan Plateau Research, Chinese Academy of Sciences, Shuangqing Road 18, Beijing 100085, China*

[2]*Key Laboratory of Western China's Environmental Systems (Ministry of Education of China) and College of Resources and Environment, Lanzhou University, Gansu 730000, China*

[3]*Key Laboratory of Continental Dynamics of the Ministry of Land and Resources, Institute of Geology, Chinese Academy of Geological Sciences, Beijing 100037, China*

**Corresponding author (e-mail: fangxm@itpcas.ac.cn)*

**Abstract:** Most existing tectonic models suggest Pliocene–Quaternary deformation and uplift of the NE Tibetan Plateau in response to the collision of India with Asia. Within the NE Tibetan Plateau, growth of the terranes was suggested to progress northeastward with the Yumu Shan (mountain) at the northeasternmost corner of the Qilian Shan (mountains) being uplifted only since about 1 Ma ago. Here we present a detailed palaeomagnetic dating and tectonosedimentological measurement of Cenozoic sediments in the eastern Jiuquan Basin related to the deformation and uplift of the North Qilian Shan and Yumu Shan. The results show that the eastern Jiuquan Basin is a Cenozoic foreland basin and received sediments at about 27.8 Ma at the latest. Eight subsequent tectonic events at about 27.8, 24.6, 13.7–13, 9.8–9.6, 5.1–3.6, 2.8–2.6, 0.8 and 0.1 Ma demonstrate the development of the foreland basin in response to Oligocene–Quaternary uplift of the North Qilian Shan and subsequent propagation of thrust–fold system owing to collision of India with Asia. The Yumu Shan is the late phase of deformation front in the thrust–fold system and commenced rapid uplift at about 9.8–9.6 Ma at the latest. A rigid block-floating model is proposed to interpret the mechanism of this deformation and uplift history.

The NE Tibetan Plateau is the furthest topographic and deformation edge of the Tibetan Plateau and is characterized by the overall features of WNW-trending ranges (Qilian Shan) and basins (Hexi to Qaidam) with high topographic reliefs (*c*. 4000–5000 m) and no Cenozoic volcanism, all truncated by the *c*. 1500 m long ENE-trending lithospheric strike-slip fault, the Altun fault (Fig. 1). This contrasts with the main Tibetan Plateau between the Himalayas and the Kunlun Shan, where a vast flat surface with widespread north–south-trending normal faults and grabens and Cenozoic volcanism occurs (Molnar & Tapponnier 1975; Fielding *et al.* 1994).

How and when these tectonomorphological features formed is less directly dealt with by many tectonic models of Tibet formation, because most working models are based on observations and data mainly from the southern edge (Himalayas–Gangdese) and in part from southern and central Tibet (e.g. Ni & Barazangi 1984; England & Houseman 1986, 1989; Dewey *et al.* 1988; Harrison *et al.* 1992; Molnar *et al.* 1993); few data have come from the remote northeastern edge of Tibet. So far only two groups of end models based on recognition of the nature of the lithosphere have provided some information on the evolution of the NE Tibetan Plateau.

The first group regards the Asian lithosphere as a thin viscous sheet, which was continuously, broadly and homogeneously thickened on India–Asia collision. Convection removal of the thickened Asian lithospheric mantle root under Tibet led to rapid and uniform isostatic rebound of the vast Tibetan Plateau to an elevation higher than the present level (*c*. 5000 m). Subsequent gravity collapse gave rise to widespread east–west extensions (manifested as north–south directed normal faults and grabens) and volcanism (England & Houseman 1986, 1988, 1989) and associated Asian monsoon onset (Molnar *et al.* 1993). Dating these events has constrained this wholesale uplift, which occurred in the Late (Harrison *et al.* 1992; Molnar *et al.* 1993) or Middle Miocene (Turner *et al.* 1993;

*From*: JOVANE, L., HERRERO-BERVERA, E., HINNOV, L. A. & HOUSEN, B. A. (eds) 2013. *Magnetic Methods and the Timing of Geological Processes*. Geological Society, London, Special Publications, **373**, 149–171. First published online November 15, 2012, http://dx.doi.org/10.1144/SP373.5 

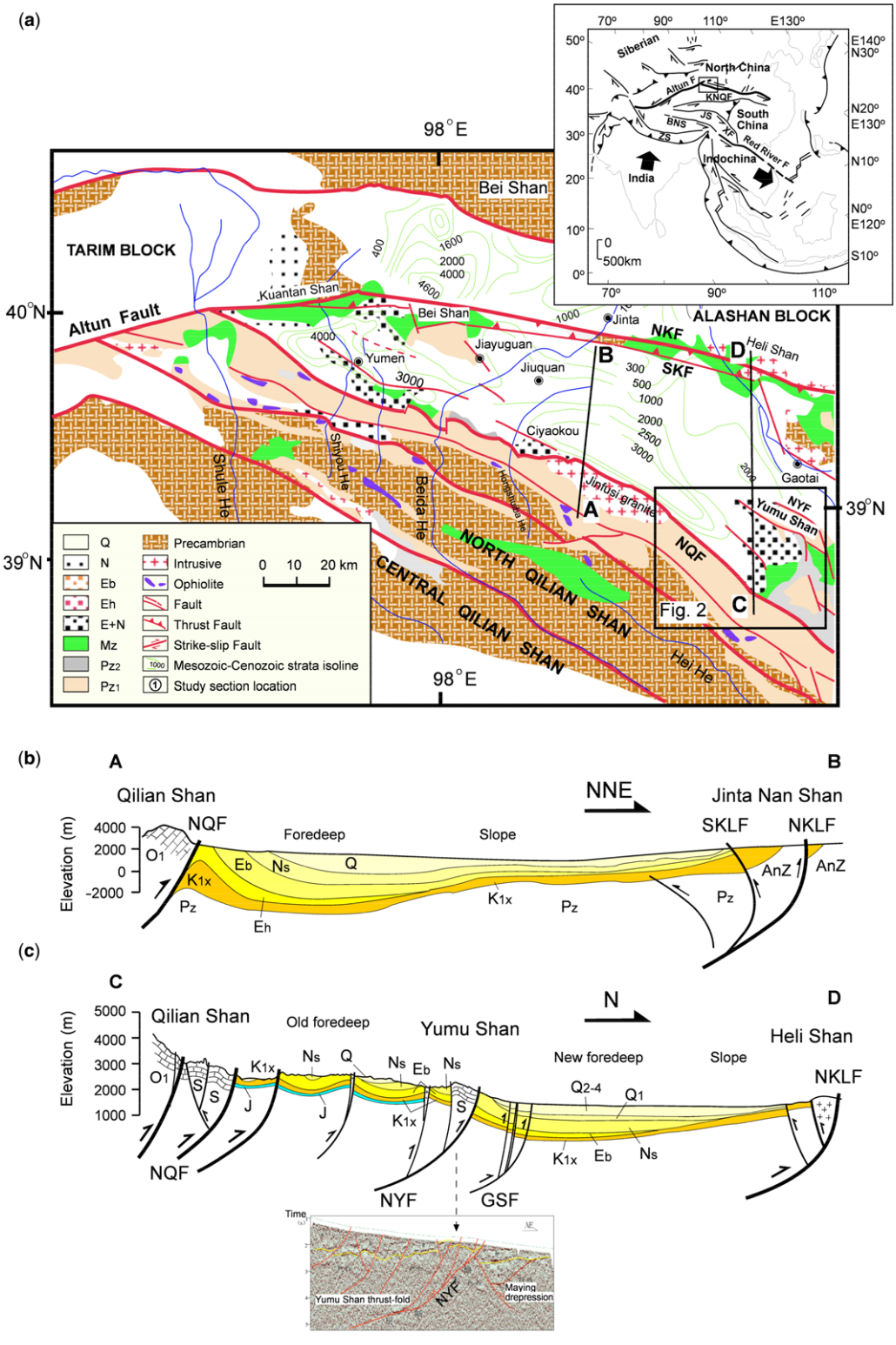

Coleman & Hodges 1995) or earlier (Chung *et al.* 1998). This model focuses on interpretation of first-order features of flatness, grabens and volcanism of the vast area north of Himalayas and south of Kunlun Shan, regarding the NE Tibetan Plateau only as a northern boundary of the model. From this model, the isostatic rebound of Tibet would have caused strong coeval activations of the northeastern boundary edge.

This group of models is derived from the hypothesis that distributed and continuous creep deformation occurs only in the lower crust (Royden 1996). Such lower crust flow moves progressively northwards and eastwards with the India–Asia collision and a later phase of deformation and uplift of the north and east margins of Tibet would be predicted (Royden *et al.* 1997, 2008).

The second group of end models regards the Asian lithosphere as rigid blocks, which were progressively broken along some former suture zones in Tibet and then squeezed out eastwards along some newly formed large lithospheric slip faults at the Tibet margin in response to the India–Asia collision, leading to northeastward oblique stepwise rise and growth of the Tibetan Plateau (Meyer *et al.* 1998; Tapponnier *et al.* 2001). South Tibet was raised with great eastward extrusion along the Red River fault in the Eocene; central-north Tibet slipped eastwards along Jinshajiang suture–Xianshuihe fault and Kunlun fault, and uplifted in the Oligocene–Miocene; and NE Tibet was extruded and grew northeastwards along the Altun fault in the Plio-Quaternary (Meyer *et al.* 1998; Tapponnier *et al.* 2001; see Fig. 1 insert for locations). Within NE Tibet, as the Altun fault propagates northeastwards, the upper crust of the NE Tibet is progressively decoupled from the Asian lower crust and mantle dipping and moving southwards beneath the Kunlun Shan (Burchfiel *et al.* 1989; Tapponnier *et al.* 1990), causing northeastward stepwise rise of the south, central and north Qilian Shan in the Plio-Quaternary and the northeastmost Yumu Shan at *c.* 1 Ma (see Fig. 15c in Tapponnier *et al.* 1990, 2001; Metiver *et al.* 1998; Meyer *et al.* 1998; Fig. 1).

Therefore, these models outlined above can be used to test the timing and processes that formed the present macrofeature of the NE Tibetan Plateau, and will provide help in understanding the dynamic mechanism of the Tibetan Plateau formation and continental deformation. The timing of deformation events holds the key.

For late-phase deformation and uplift of NE Tibet predicted from the models above, fission track analysis shows that the Qilian Shan experienced a rapid cooling in the Miocene (George *et al.* 2001; Jolivet *et al.* 2001), and some preliminary palaeomagnetic work shows that the Danghe Nan Shan (South Qilian Shan) and western North Qilian Shan may have uplifted in the Eocene or Oligocene (Yin *et al.* 2002; Dai *et al.* 2005). Recent U–Th/He dating of rocks in the central East Kunlun Shan (mountains) and West Qinling (mountains) and basin sedimentological analysis indicate an Eocene to Oligocene deformation and uplift of the NE Tibetan Plateau (Clark *et al.* 2010; Zhang *et al.* 2010; Fang *et al.* 2003). Our previous high-resolution palaeomagnetic dating of the Laojunmiao section in Yumen in the western Jiuquan Basin provided the first detailed time constraint for the late Cenozoic stratigraphy and demonstrated that the western North Qilian Shan was rapidly uplifted at latest about 8 Ma (Fang *et al.* 2005*b*). These studies show the lack of consensus and call for more detailed work to identify the precise timing of the Cenozoic deformation and uplift history of the Qilian Shan. Here we present a detailed palaeomagnetic dating and tectonosedimentological analysis of Cenozoic sediments in the margins of the Yumu Shan to test if the mountain was the most recently (*c.* 1 Ma) uplifted part of the NE Tibetan Plateau as predicted by the commonly accepted model of Tapponnier's group (Tapponnier *et al.* 1990, 2001; Meyer *et al.* 1998; Metiver *et al.* 1998).

## Geological setting and stratigraphy

The NE Tibetan Plateau is a terrane delineated by the major sinistral Kunlun–North Qinling strike-slip fault in the south, the Altun fault to the west and the North Qilian–Haiyuan–Liupan Shan fault in the north and east (Fig. 1). From SW to NE, it consists of Qaidam Basin, Qilian Shan, Longzhong Basin and Liupan Shan. The Qilian Shan is

**Fig. 1.** Geological and location map of the Qilian Shan and Hexi Corridor Basin (**a**). Note that the basin-cross sections (**b** and **c**) show the nature of a foreland basin owing to compressive flexure and the northward migration of the foredeep owing to uplift of the Yumu Shan (c; data were provided by Yumen Oil Field Co.). NQF, North Qilian fault; NCQF, northern marginal fault of Central Qilian Shan; NKLF, northern marginal fault of Kuantan Shan–Longshou Shan; SKLF, southern marginal fault of Kuantan Shan–Longshou Shan; NYF, northern Yumu Shan fault; KNQF, Kunlun–North Qinling fault; XF, Xianshuihe fault; JS, Jinshajiang suture; BS, Bangong suture; ZS, Zangbo suture. $O_1$, Early Ordovician; S, Silurian; J, Jurassic; $K_{1x}$, Early Cretaceous Xiagou Formation; $E_b$, Palaeogene Baiyanghe Formation; $N_s$, Neogene Shulehe Formation; $Q_1$, Early Quaternary; $Q_{2-4}$, Late Quaternary.

of interest in this study, and consists of south, central and north Qilian Shan. The Yumu Shan is the northeasternmost corner of the North Qilian Shan (Fig. 1).

The Qilian Shan orogenic belt formed in the Caledonian through collisions of Proterozoic south and central Qilian terranes with North China block and Eastern Kunlun–Qaidam terrane, mostly in the Silurian (see Fig. 1 inset for locations). Subsequent tectonic movements in response to collisions of older Tibetan terranes (Qiangtang and Lhasa) in the Tethys Sea with Palaeo-Asia (here southern margin of Eastern Kunlun–Qaidam terrane) resulted in relatively minor modification of the existing structural setting. The sea receded completely from the North Qilian Shan from the Middle Permian (Gansu Geologic Bureau 1989; Feng & Wu 1992; Yin & Harrison 2000; Fig. 2). The purpose of this paper is to examine the last rejuvenation (uplift) of the Qilian Shan caused by remote response to the collision of the Indian block with Palaeo-Asia (here the southern margin of the Lhasa terrane) in the Neotethys Sea.

The southern and central Qilian terranes and Alashan Block consist mainly of very thick (>15 km) basement rocks of Proterozoic gneisses, schists, slates, phyllite, dolomite and limestones, intercalated with some quartzite, chert, shales, migmatite, tuff and basalt. Early Palaeozoic and Silurian–Devonian stratigraphy were absent from these terranes, with only a small amount of Middle Cambrian and Lower and Middle Ordovician marine limestone and clasts deposited in marginal areas. The cover rocks are mainly Carboniferous–Triassic neritic and paralic clast and carbonates, intermontane Jurassic coal-bearing sediments and Cretaceous–Quaternary clast and molasse (Gansu Geologic Bureau 1989; Feng & Wu 1992; Fig. 2).

The North Qilian Shan is composed mainly of Cambrian–Devonian stratigraphy and Caledonian granite and diorite, which form the core of the mountain. Carboniferous to Quaternary stratigraphy is restricted mostly along the northern margin of the core. The Cambrian–Ordovician rocks form the base of the North Qilian Shan and are mainly basic–intermediate volcanic and pyroclastic rock, chert, phyllite and slate, recording the Qilian ocean history (Fig. 2). The Silurian consists of low-grade metamorphosed continental flysch consisting of purple sandstone and phyllite, representing the closure of the Qilian Ocean. The Devonian is a molasse sequence of post-orogenic purple conglomerates and sandstones. The Carboniferous and Lower Permian are neritic and paralic grey, green sandstone, carbonaceous shale and limestone intercalated with some coal beds. The Upper Permian consists of continental purple conglomerate and sandstone, recording the complete emergence of the region from the sea (Fig. 2). The Triassic to Cretaceous are intermontane multi-coloured (green, yellow-green, blue, grey, purple-grey, purple, brown) sandstone and conglomerate, intercalated with carbonaceous shale, coal and mudstone (Gansu Geologic Bureau 1989; Feng & Wu 1992; Fig. 2).

The Yumu Shan is an independent massif located to the north of the North Qilian Shan uplifted on the North Yumu Shan progradation fault (NYF; Tapponnier *et al.* 1990; Fig. 1c). It comprises mainly Silurian sedimentary rocks and small proportions of other Palaeozoic and Mesozoic rocks having the same lithology as those in the North Qilian Shan (Gansu Geologic Bureau 1971; Figs 3 & 4).

To the north of the Qilian lies the Alashan Block and its marginal mountains of Kuantan Shan–Bei Shan–Longshou Shan, consisting of Proterozoic rocks similar to those in the Qilian Shan (Gansu Geologic Bureau 1989; Feng & Wu 1992; Figs 1 & 2).

Between the Qilian Shan and the Alashan Block is the long and narrow Hexi Corridor Basin, a Cenozoic foreland basin developed atop a Jurassic foreland basin (Wang & Coward 1993) with its base as a passive continental margin of the Alashan Block (Feng & Wu 1992; Fig. 2), or developed on Early Cretaceous extensive basins in the front of these mountains (Gansu Geologic Bureau 1989; He *et al.* 2004). This foreland basin is divided from NW to SE into Jiuquan, Zhangye and Wuwei sub-basins by several NNW dextral faults and their related uplands in the Yumu Shan and the Dahuang Shan (EGPGYO 1989; Fang *et al.* 2005*b*). The studied sections are located in the east end of the Jiuquan Basin surrounded by the North Qilian Shan, Altun fault, Kuantan Shan and Yumu Shan to the south, west, north and east, respectively (Figs 1 & 3).

Thick Cenozoic stratigraphy is deposited in the Hexi Corridor Basin and its distribution is strictly controlled by faults. Cenozoic stratigraphy is exposed only north of the Northern Qilian fault and south of the southern marginal fault of Kuantan Shan–Longshou Shan. Stratigraphy thickness is over 3000 m in proximity to the North Qilian Shan and gradually thins northwards to <300 m in the southern foot of the Longshou Shan, presenting a typical foreland basin clastic wedge (Fig. 1a, b). Within the basin, several propagation faults control some new foredeep formation and sedimentary deposition, which caused a second depocentre in the new foredeep. This is quite obvious in the western part of the Jiuquan Basin (not shown by cross section in our Fig. 1 owing to space limit, but can be seen on Fig. 1 in Fang *et al.* 2005*b*). North of the Yumu Shan in the eastern end of the Jiuquan Basin, the northern Yumu Shan fault clearly controls a new foredeep and deposition of the Neogene Shulehe Formation and Quaternary sediments to the north of the fault (Fig. 1c). Isobath lines obtained from boreholes and seismostratigraphy of PetroChina demonstrate clearly a second depocentre of the

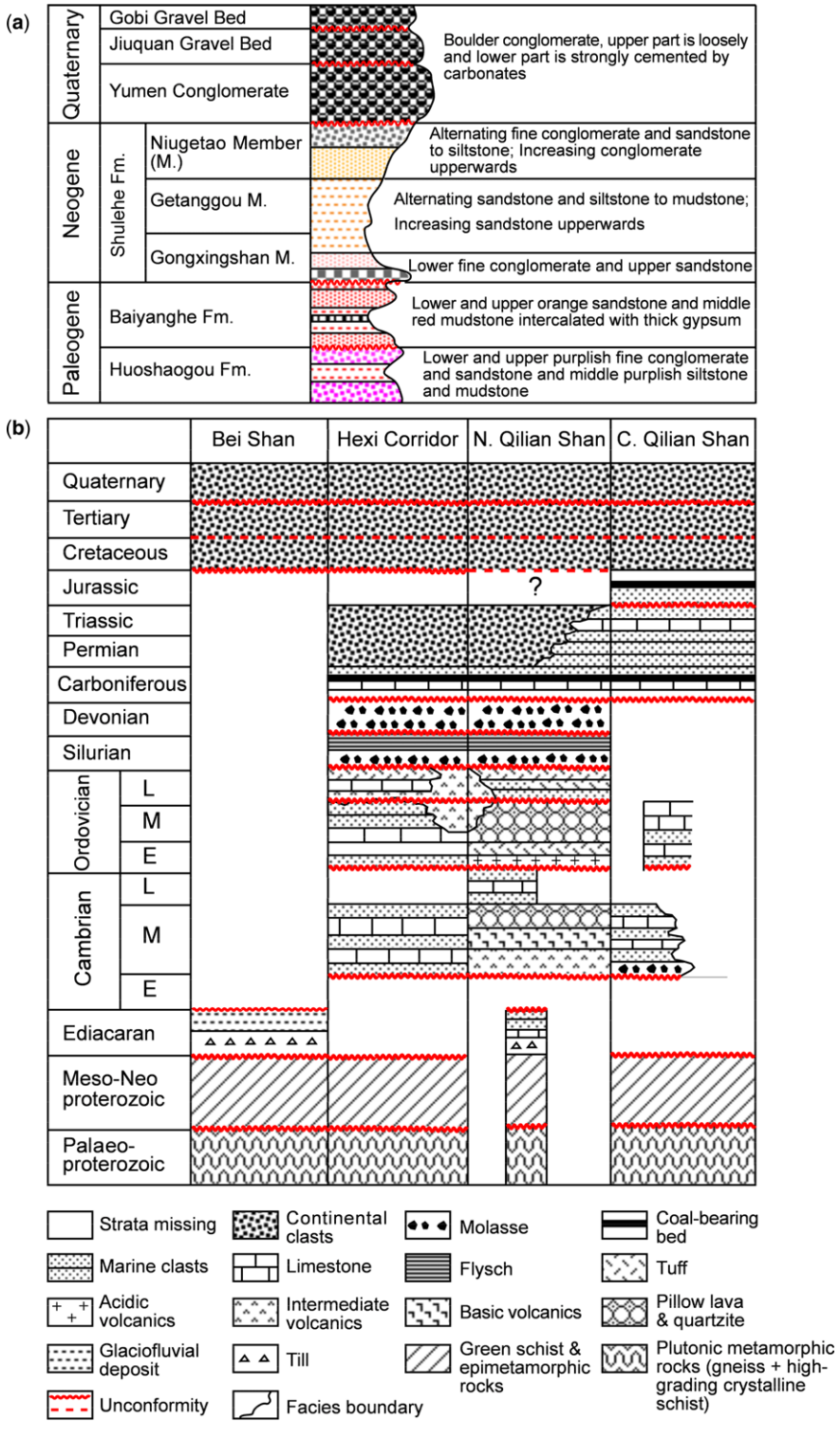


**Fig. 2.** Tectonostratigraphic evolution of the studied region.

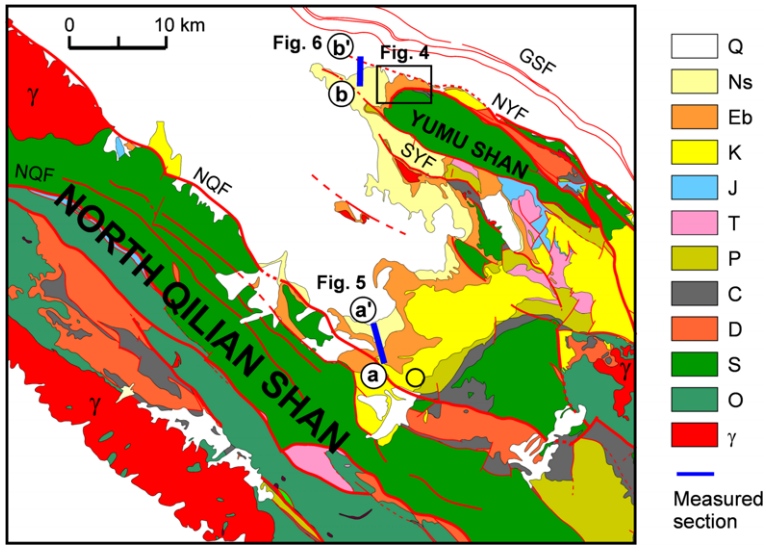


**Fig. 3.** Geological map of the Yumu Shan and North Qilian Shan showing domination of Palaeozoic rocks and Caledonian granite and locations of two studied sections. Note that the distribution of the Oligocene stratigraphy of the Baiyanghe Formation extends into the North Qilian Shan. NQF, Northern Qilian fault; NYF, northern Yumu Shan fault; SYF, southern Yumu Shan fault; GSF, Gaotai Station fault. T, Triassic; P, Permian; C, Carboniferous; D, Devonian; γ, Caledonian granites. Other stratigraphic units are same as in Figure 1.

Cenozoic stratigraphy appearing in the front of the northern Yumu Shan fault (Fig. 1a).

The Cenozoic stratigraphy consists upwards of Palaeogene Huoshaogou Formation (Eh) and Baiyanghe Formation (Eb) of alluvial and fluviolacustrine red beds of fine conglomerate to mudstone intercalated with some playa gypsum beds, Neogene Shulehe Formation (Ns) of alternated fluviolacustrine grey and brown fine conglomerate, sandstone and siltstone, and Quaternary Yumen Conglomerate Bed (Yumen Formation, $Q_1$), Jiuquan Gravel Bed (Jiuquan Formation, $Q_2$) and Gobi Gravel Bed (Gobi Formation, $Q_{3-4}$; Figs 2 & 3). The Huoshaogou Formation is only distributed in the proximity to the North Qilian Shan and Kuantan Shan–Longshou Shan (Fig. 1; Gansu Geologic Bureau 1989; EGPGYO 1989; Dai *et al.* 2005; Fang *et al.* 2005*b*). The studied area only has the Cenozoic stratigraphic sequence from the Baiyanghe Formation, which is superimposed unconformably on the Lower Cretaceous rocks (Gansu Geologic Bureau 1971). This sequence is completely exposed in folds in the fronts of the North Qilian Shan and Yumu Shan (Figs 1 & 3).

## Studied sections

Two sections were chosen for detailed measurements and sampling. One is located on the southern limb of the Sunan syncline between the North Qilian Shan and the Yumu Shan, called the Sunan section (3853′54.9″N, 99°35′39.6″E), the other on the outer part of the northern limb of the Yumu Shan anticline, called the Upper Yumu Shan section (39°15′19.43″N, 99°29′46.13″E; Figs 1c & 3).

The Sunan section is 916 m thick and exposes the Baiyanhe Formation and the Shulehe Formation (Fig. 5). An angular unconformity (U1) exists between the Baiyanhe Formation and the underlying Cretaceous Ximinpu Group. The Baiyanhe Formation (from 0 to 272 m) consists predominantly of fine-grained distinct red-orange, brownish red and purple mudstones and sandstones, intercalated with thin fine-grained grey conglomerate layers. It contains a characteristic thick sandy gypsum bed near the bottom (Fig. 5). The Shulehe Formation (from 272–916 m) is an upward coarsening sequence with the lower part consisting of alternating layers of grey conglomerate and yellow-brown mudstone and siltstone, and the upper part of predominant thick grey conglomerate layers, intercalated with thin brownish yellow sandstone and siltstone lenses. An angular unconformity exists between the Baiyanghe and Shulehe Formations (U2). Growth strata exist at the bottom of the Shulehe Formation, with strata dip shallowing from 25 to 18° between 272 and 343 m (Fig. 5).

The Upper Yumu Shan section contains sediments from the Beiyanghe Formation to the Quaternary (Figs 3 & 4), but it is complicated by


**Fig. 4.** Southeastern view of the western Yumu Shan and the Cenozoic stratigraphy in the Lower Yumu Shan section. Note that the Yumu Shan thrusts over the Cenozoic stratigraphy along the North Yumu Shan fault (NYF). See Figure 2 for location.

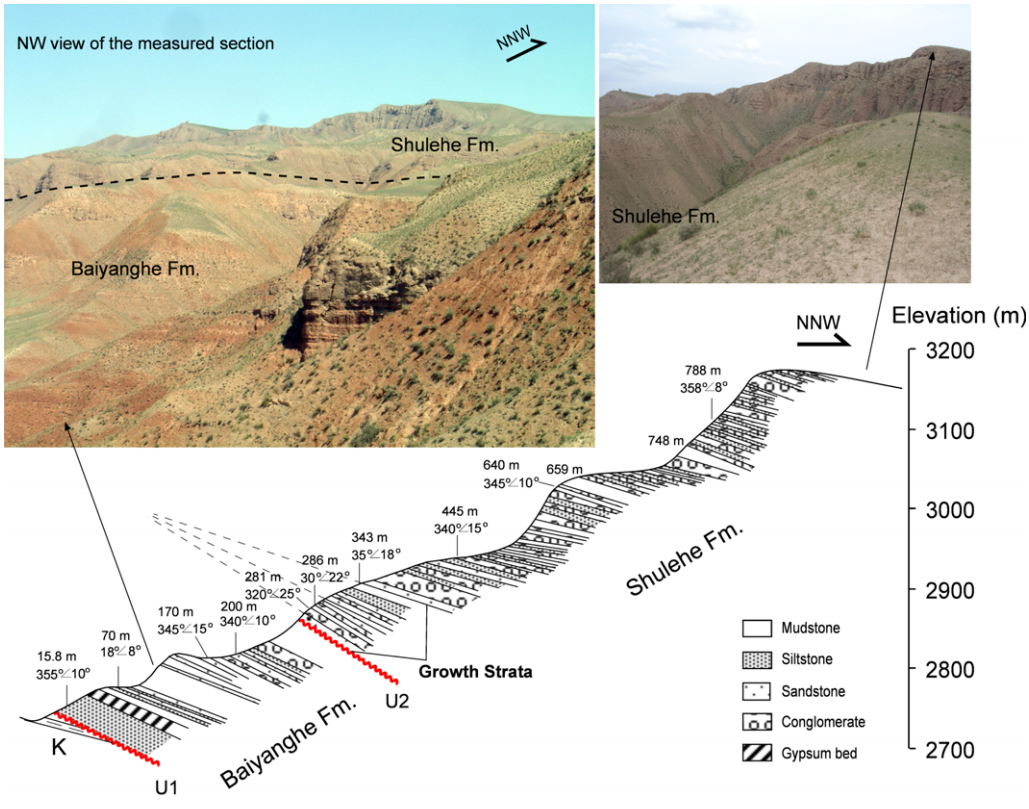


**Fig. 5.** The measured Sunan section along the southern limb of the Sunan syncline between the North Qilian Shan and the Yumu Shan. See Figures 1*c* and 2 for location.

many faulted and buried segments owing to close proximity to the Yumu Shan, and thus is not suitable for main palaeomagnetic dating. Only the uppermost part of this section was studied to supplement the Sunan section. The measured Upper Yumu Shan section is 400 m thick. Its bottom part consists of 69 m of the uppermost Shulehe Formation, characterized by interbedded thin yellow–grey fine conglomerate and sandstone. Its middle and upper parts are all thick layers of Quaternary greyconglomerates intercalated with some thin yellowish sandstone and siltstone lenses, with gravel diameter coarsening upwards. Four unconformities (U3–U6) occur at thicknesses 69, 148, 296 and 400 m, dividing the Quaternary conglomerates respectively into the Lower and Upper Yumen Conglomerate Beds, the Jiuquan Gravel Bed and the Gobi Gravel Bed (unmeasured; Fig. 6).

## Sampling and laboratory measurements

Within the two measured sections, orientated block samples of about 10 × 10 × 8 cm in size were taken at intervals of 1–2 m in the mudstone and sandstone layers, and *c.* 3–4 m in the conglomerate layers, depending on the occurrence of sandstone and siltstone lenses. Each oriented sample was cut into three cubic specimens of 2 × 2 × 2 cm in size in the laboratory. A total of 630 block samples and 1890 specimens were obtained.

According to previous studies in this region, thermal demagnetization provides better results than alternating field demagnetization, as the magnetization carrier is mostly hematite (Dai *et al.* 2005; Fang *et al.* 2005*b*). We only used thermal demagnetization analysis in this study. The samples were measured on a 2 G magnetometer in a magnetically sheltered room in the Paleomagnetism Laboratory of the Institute of Geology and Geophysics, Chinese Academy of Sciences.

Eighteen systematic stepwise thermal demagnetizations were carried out for pilot samples from different lithologies and layers, from room temperature to 680 °C with intervals of 10–50 °C. Representative thermal demagnetization diagrams show that most samples present a similar demagnetization behaviour. The low temperature component can be

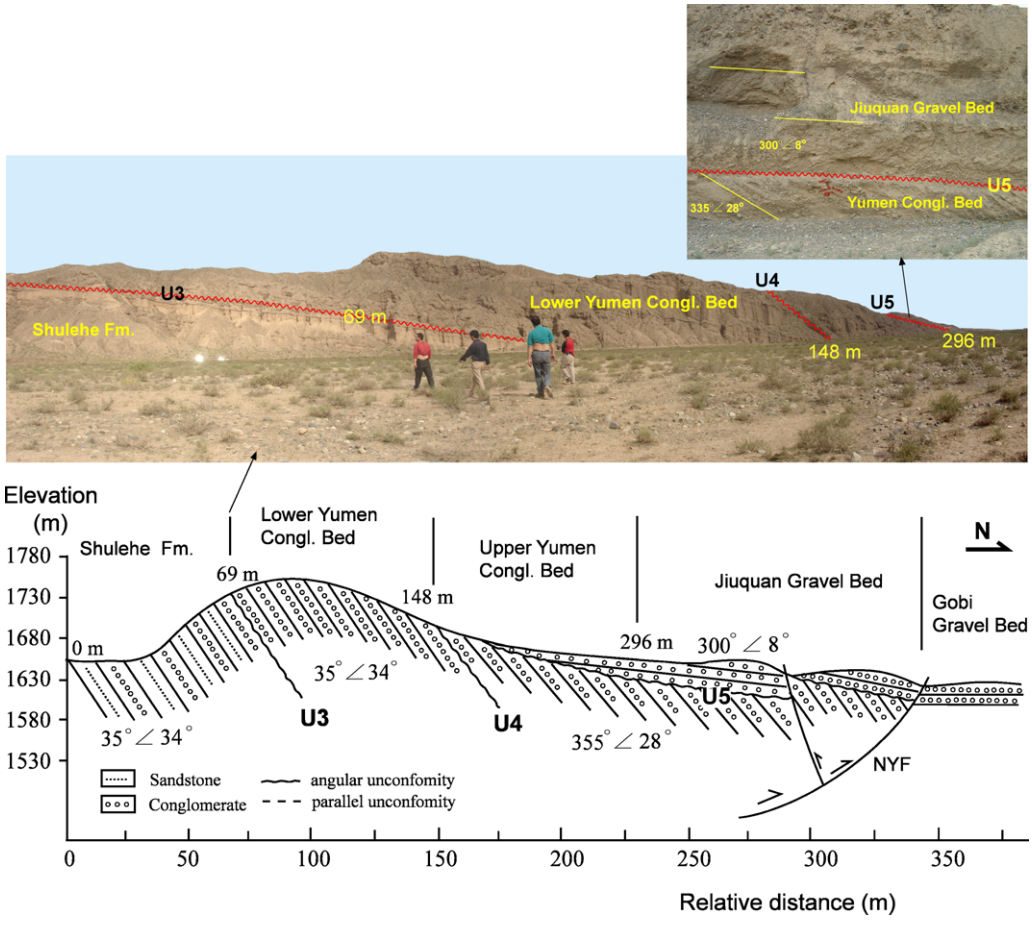


**Fig. 6.** The measured Upper Yumu Shan section showing the occurrences of unconformities in the Plio-Quaternary stratigraphy.

readily removed around 220 °C, and the characteristic remanent magnetization (ChRM) can be clearly isolated above 300 °C. An obviously rapid decay of the remanent magnetization occurs at 650–680 °C, with a small drop at around 580 °C, indicating that hematite is the major ChRM-carrier and magnetite is the second one (Fig. 7). Based on the pilot samples, the rest of the samples were measured with 12–14 steps from 300 to 680 °C. The ChRM directions were obtained by principal component analysis, and the virtual geomagnetic poles (VGPs) were then calculated. Specimens not included in the magnetostratigraphic analysis were rejected based on three criteria: (1) ChRM directions could not be determined because of ambiguous or noisy orthogonal demagnetization diagrams; (2) ChRM directions revealed maximum angular deviation angles $>15^{\circ}$; and (3) Specimens yielded magnetizations with VGP latitude values $<30^{\circ}$.

All the accepted ChRM directions of the Sunan section were used for Fisherian statistics and the reversal test. The difference between the normal and reversed mean magnetic declinations was almost 180° (353.5 v. 172.4°), and that of the normal and reversed mean inclination was around 90° (35 v. −34.4°; Fig. 8a). The statistical bootstrap technique (Tauxe 1998) was used to examine possible non-Fisherian distributions of ChRM vectors, and to characterize the associated uncertainties for both normal and reversed ChRM directions (Fig. 8c). The reversed-polarity directions were inverted to their antipodes to test for a common mean for the normal and reversed magnetization directions. The confidence intervals for all components overlap, indicating a positive reversal test (Tauxe 1998; Fig. 8c). The results in Figure 7a, c indicate that the obtained ChRMs are most likely the primary remanences.

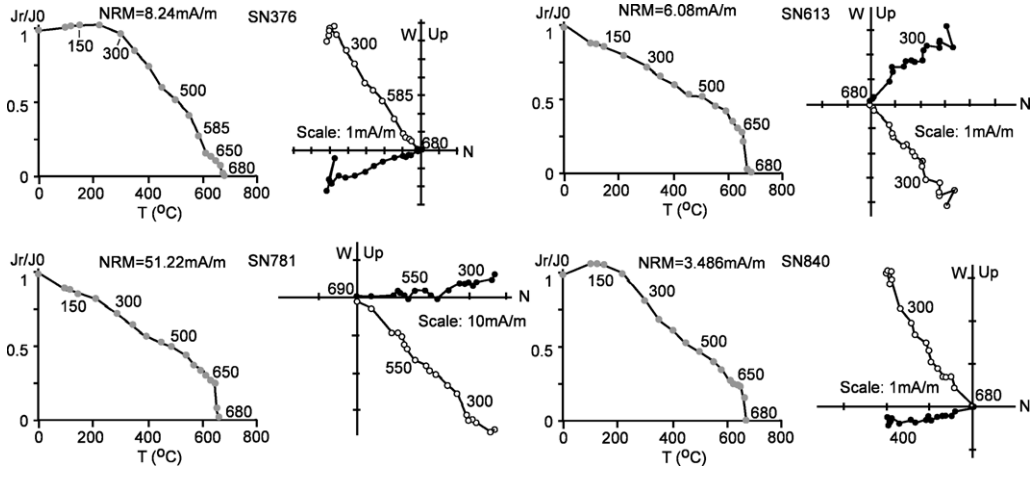


**Fig. 7.** Orthogonal presentation of thermal demagnetization of some representative samples from the Sunan section. Solid and open circles represent horizontal and vertical projections, respectively.

For the fold test, 100 representative high-quality (maximum angular deviation $<5$) site-mean ChRMs from different parts of the section were averaged again to fall into 11 grouped sites according to stratigraphic dip and were used for a calculation by the method of McElhinny (1964), which indicates a positive fold test with the tilt-dependent dispersed ChRM directions tending to cluster together around their antipolar means (Fig. 9).

## Magnetostratigraphy

The VGP results were plotted as a function of thickness for the Sunan section. We regarded single VGP direction as the unstable or unreliable direction, and thus it was not included in the magnetic zone for interpretation. A total of 22 normal (N1–N22) and 22 reversed (R1–R22) polarity zones are clearly observed in the section (Fig. 10). Palaeontological findings in the Jiuquan Basin were used to control the magnetostratigraphic interpretation.

Many fossil mammals have been found in the upper and middle parts of the Baiyanghe Formation in sites near our section and throughout the Jiuquan Basin (Fig. 10). These include *Tataromys grangeri*, *T. Sigmoden*, *Leptotataromys minor*, *Parasminthus* cf. *Asiae-centralis*, *P. tangingili*, *P. parvulus*, *Eucricetodon asiaticus*, *Desmatolagus* sp., *Sinolagomys* sp. and *Amphechinus* sp. All of these fossils are major components of the Chinese Taben buluk fauna, which lived during late Oligocene time (Wang 1965; Exploration and Exploitation Department of the Yumen Oilfield, 1990, 'The Tertiary in the Jiuquan Basin', unpublished). Furthermore, fossils of stoneworts (*Tectochaea*, *Kosmogyra ovalis* and *Charites huangi* sp.), ostracods and gastropods (*Metacypris* sp., *Ostrea* sp., *Nyocypris* sp., *Chara* sp., *Plannorbis* sp., *Hydrobia* sp. and *Ancykes* sp.) were found in the lower and middle parts of the Shulehe Formation, suggesting a Miocene age (Wang 1965; Exploration and Exploitation Department of the Yumen Oilfield, 1990, 'The Tertiary in the Jiuquan Basin', unpublished).

Based on the above age constraints, the observed chrons in the Baiyanghe Formation can be correlated with the GPTS chrons between 6Cr and 9n (Cande & Kent 1995), with the prominent two long normal polarity zones N21 and N20 correlating with the characteristic long normal chrons 9n and 8n, and N17 with 7n (Fig. 10). The 16 observed normal (N1–N16) and 17 reversed chrons (R1–R17a) in the Shulehe Formation match well with the GPTS chron interval between 4Ar and 5ABr. The distinct long, mostly normal zone interval (N2–N6) is correlated with striking long normal chron of 5n, with short reversed zones R3–R6 being regarded as analogues of several cryptochrons in chron 5n (Cande & Kent 1995; Fig. 10). These cryptochrons are frequently recorded in chron 5n in the NE Tibetan Plateau (Li *et al.* 1997; Fang *et al.* 2005*a*, *b*), nearby regions (Charreau *et al.* 2009) and other parts of the world (Cande & Kent 1995; Garćes *et al.* 1996). The normal zones N11–N16 can be correlated with Chrons 5An–5ABn. We correlated the mostly reversed zone interval (R7–R11) with the long striking reversed chron of 5r, and the two short normal zones N7 and N8 with the short normal chrons of 5r.1n and 5r.2n, and regarded other two short normal zones N9 and N10 as false signals probably owing to non-fresh samples in the section (Fig. 10).

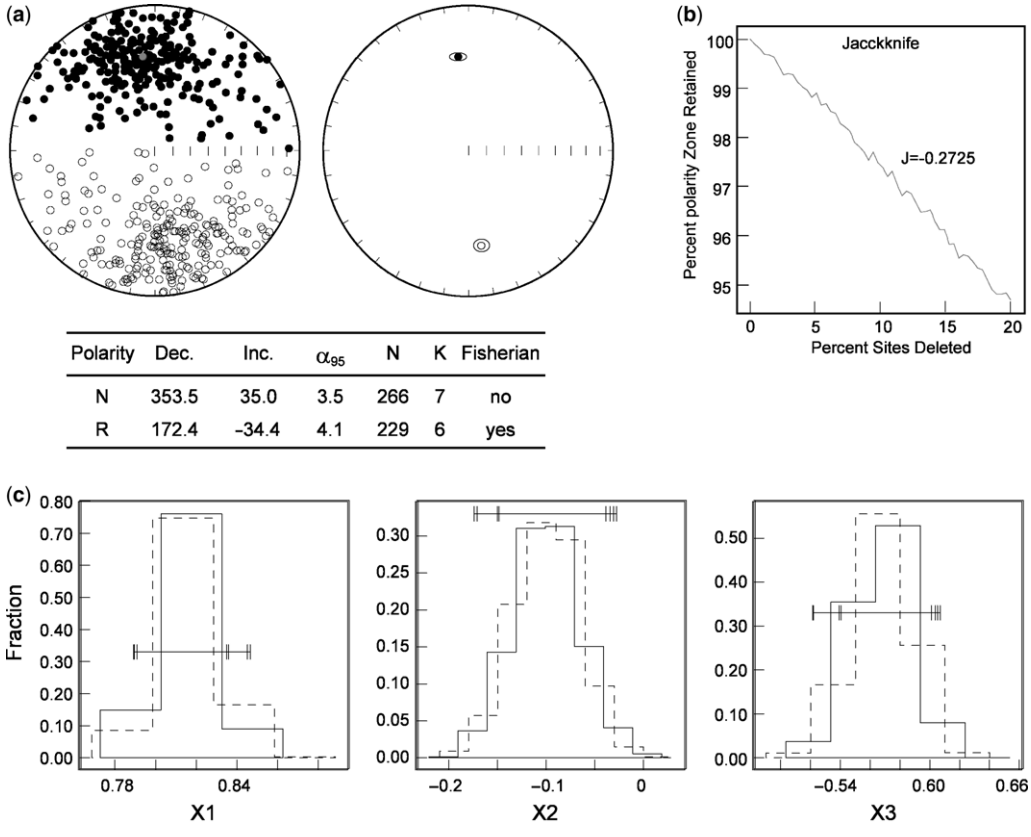


| Polarity | Dec. | Inc. | $\alpha_{95}$ | N | K | Fisherian |
|---|---|---|---|---|---|---|
| N | 353.5 | 35.0 | 3.5 | 266 | 7 | no |
| R | 172.4 | -34.4 | 4.1 | 229 | 6 | yes |

**Fig. 8.** (**a**) Equal-area projections of the obtained ChRM directions and mean directions (with oval of 95% confidence and their Fisherian statistics in the table below) for the Sunan section determined with the bootstrap method (Tauxe 1998). Downward (upward) directions are shown as solid (open) circles. (**b**) Magnetostratigraphic jack-knife analysis (Tauxe & Gallet 1991) for the Sunan section. The plot indicates the relationship between average percentage of polarity zones retained and the percentage of sampling sites deleted, where the slope *J* is directly related to the robustness of the results. The obtained slopes *J* have values of −0.2725 in the study section, which predicts that the section has recovered more than 95% of the true number of polarity intervals. (**c**) Bootstrap reversal test diagram for the Sunan section. Reversed polarity directions have been inverted to their antipodes to test for a common mean for the normal and reversed magnetization directions. The confidence intervals for all components overlap, indicating a positive reversal test.

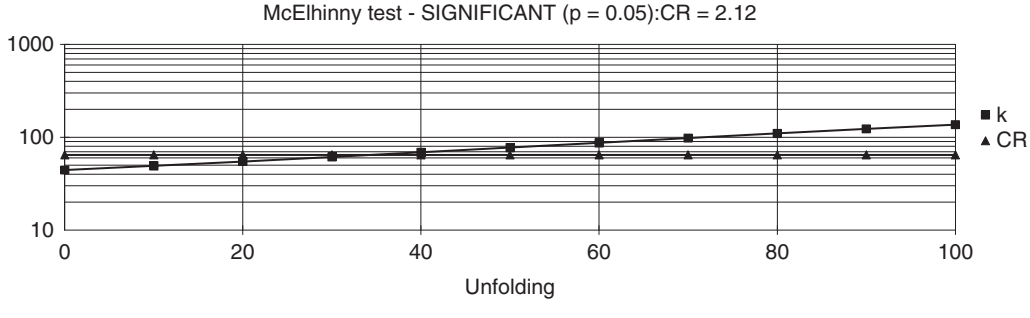


**Fig. 9.** Fold test of high-quality samples Fisher-averaged for 11 sites along different heights (and thus dips) of the Sunan section.

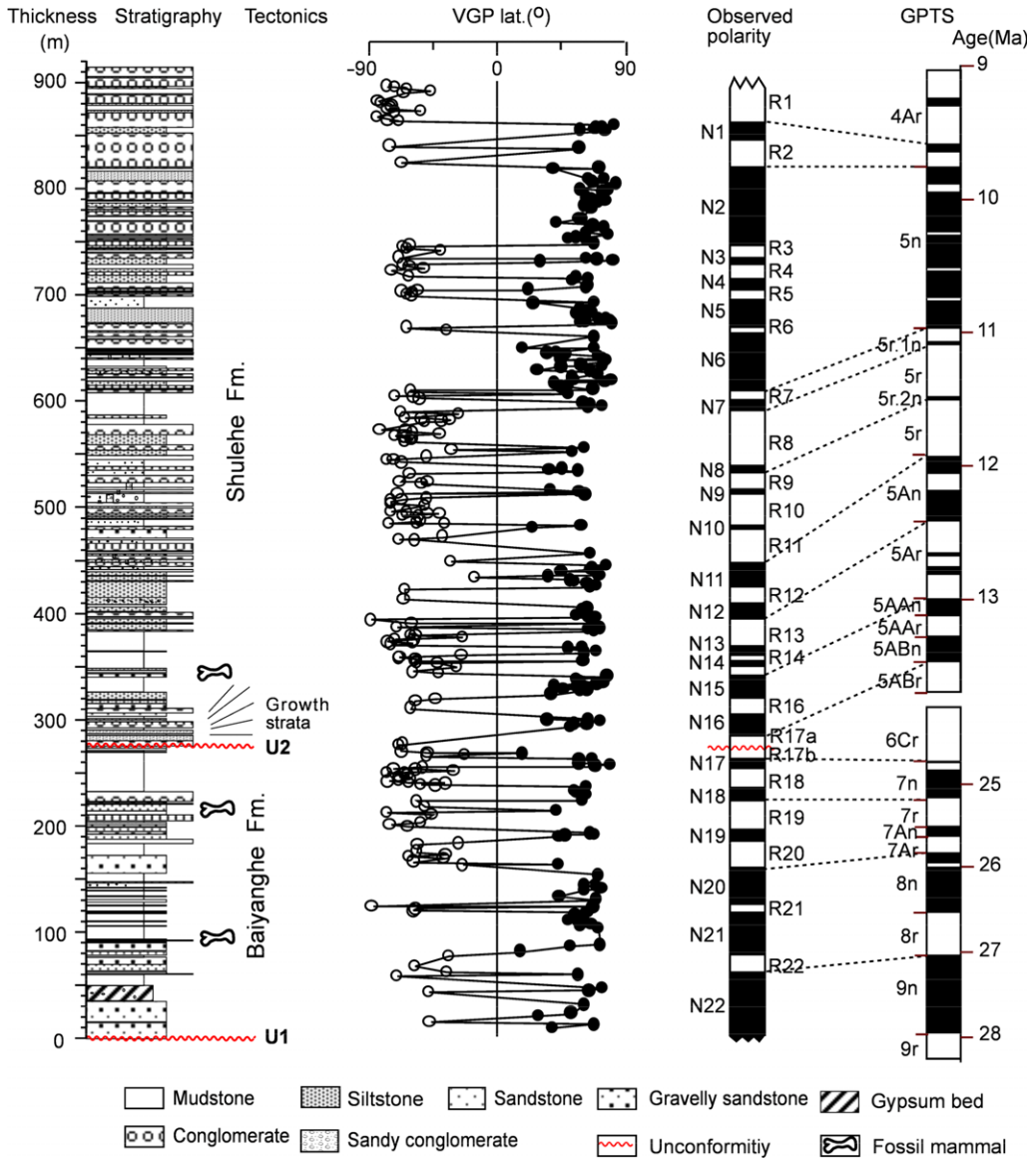


**Fig. 10.** Magnetostratigraphy of the Sunan section and its correlation with the geomagnetic polarity time scale (GPTS) of Cande and Kent (1995). VGP, Virtual geomagnetic pole. Fossil levels were roughly equivalent to those in nearby sections.

We performed a robust test for the obtained magnetostratigraphy. The jack-knife parameter ($J$) obtained for the observed polarity zones of this section has a value of $-0.2725$, which falls within the range of 0 to $-0.5$ recommended for a robust magnetostratigraphic data set by Tauxe & Gallet (1991). This result indicates that sampling of this section has recovered more than 95% of the true number of polarity intervals (Fig. 8b).

Palaeomagnetic directions and polarity zones of the Upper Yumu Shan section are plotted in Figure 9 for a whole view of the magnetostratigraphic sequence in the Yumu Shan area. Reasons for its interpretation and correlation with the GPTS were described in an earlier publication (Liu *et al.* 2010).

Based on these new data, the age of the Sunan section was constrained between about 27.8 and 9.33 Ma, with the Baiyanghe and Shulehe Formations

forming at about 27.8–24.63 and >13.69–9.33 Ma, respectively. The age of the Upper Yumu Shan section was dated between about 6.1 and 0.1 Ma, with the lower and Upper Yumen Conglomerate Beds being constrained at about 3.6–2.8 and 2.6–0.9 Ma, and the Jiuquan Gravel Bed at about 0.8–0.1 Ma (Liu *et al.* 2010; Fig. 11).

These age determinations are in good agreement with those we obtained for the Laojunmiao section at Yumen in the western Jiuquan Basin (see Fig. 1*a* for location), where the Shulehe Formation and the Yumen and Jiuquan Conglomerates were dated at >13–4.9, 3.66–0.93 and 0.84–0.14 Ma, respectively (Fang *et al.* 2005*b*). They also generally match previous preliminary magnetostratigraphic determinations of the Baiyanghe Formation at about 31.6–24.6 Ma and the Shulehe Formation at about 22.5–4.2 Ma in the Jiuquan Basin (Huang *et al.* 1993).

## Sedimentology and palaeocurrents

### *The Sunan section*

Field investigations and quantification of lithology (Fig. 12) show that the Baiyanghe Formation consists dominantly of fine-grained distinct red-orange, brown-red and purple sandstones and mudstones, intercalated with some thin fine-grained grey conglomerate layers below sandstones. In the lower part, there is a characteristic thick sandy gypsum bed (Figs 5 & 13c). The sandstones are moderately to well sorted, massive or weakly laminated and occasionally cross-bedded. The siltstone and mudstones are usually massive with rare mud cracks. Both sandstones and siltstones–mudstones contain some carbonate concretions, with some sandstones cemented by carbonates. We interpreted these as flood plain–flood basin deposits with some playa deposits formed in an arid environment (Reading 1978; Fig. 13c).

The Shulehe Formation is an upward-coarsening sequence that can be divided into three lithological units. The lower unit (272–383 m) is an up-fining sequence with a fine conglomerate and sandstone bed complex at the bottom (272–315 m; corresponding to growth strata), and mostly brown mudstones in the upper section (315–383 m; Figs 5, 12 & 13c). The conglomerates develop clear imbricate structure and parallel bedding, and the sandstones are mostly massive and occasionally

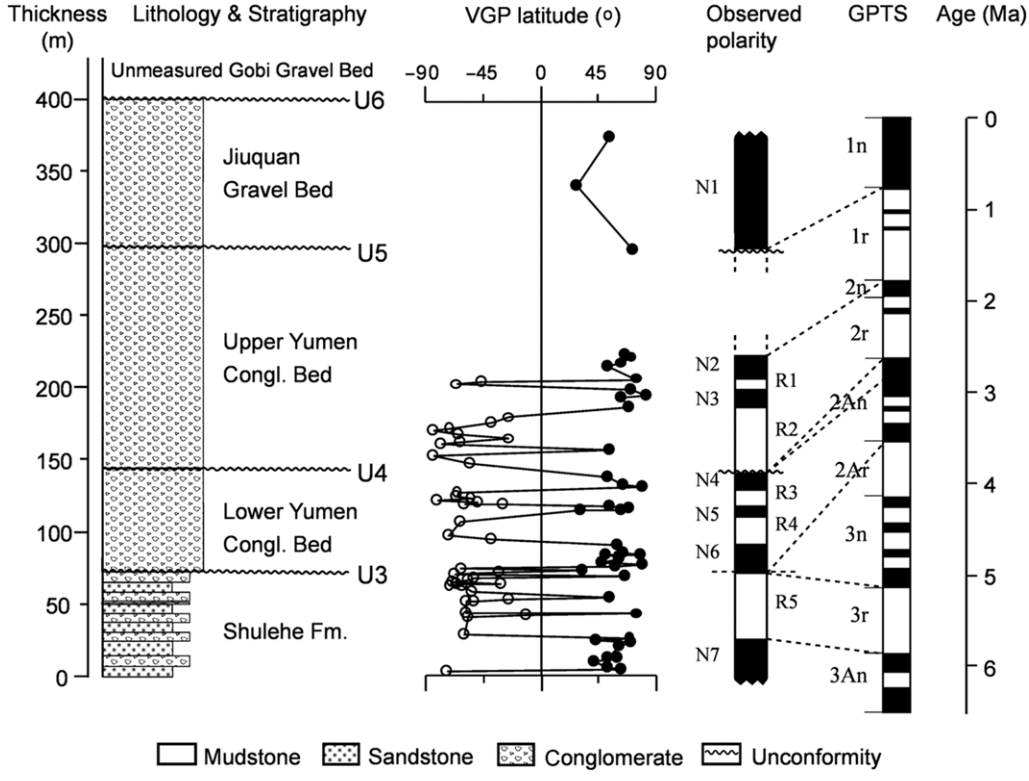


**Fig. 11.** Magnetostratigraphy of the Upper Yumu Shan section and its correlation with the GPTS of Cande & Kent (1995).

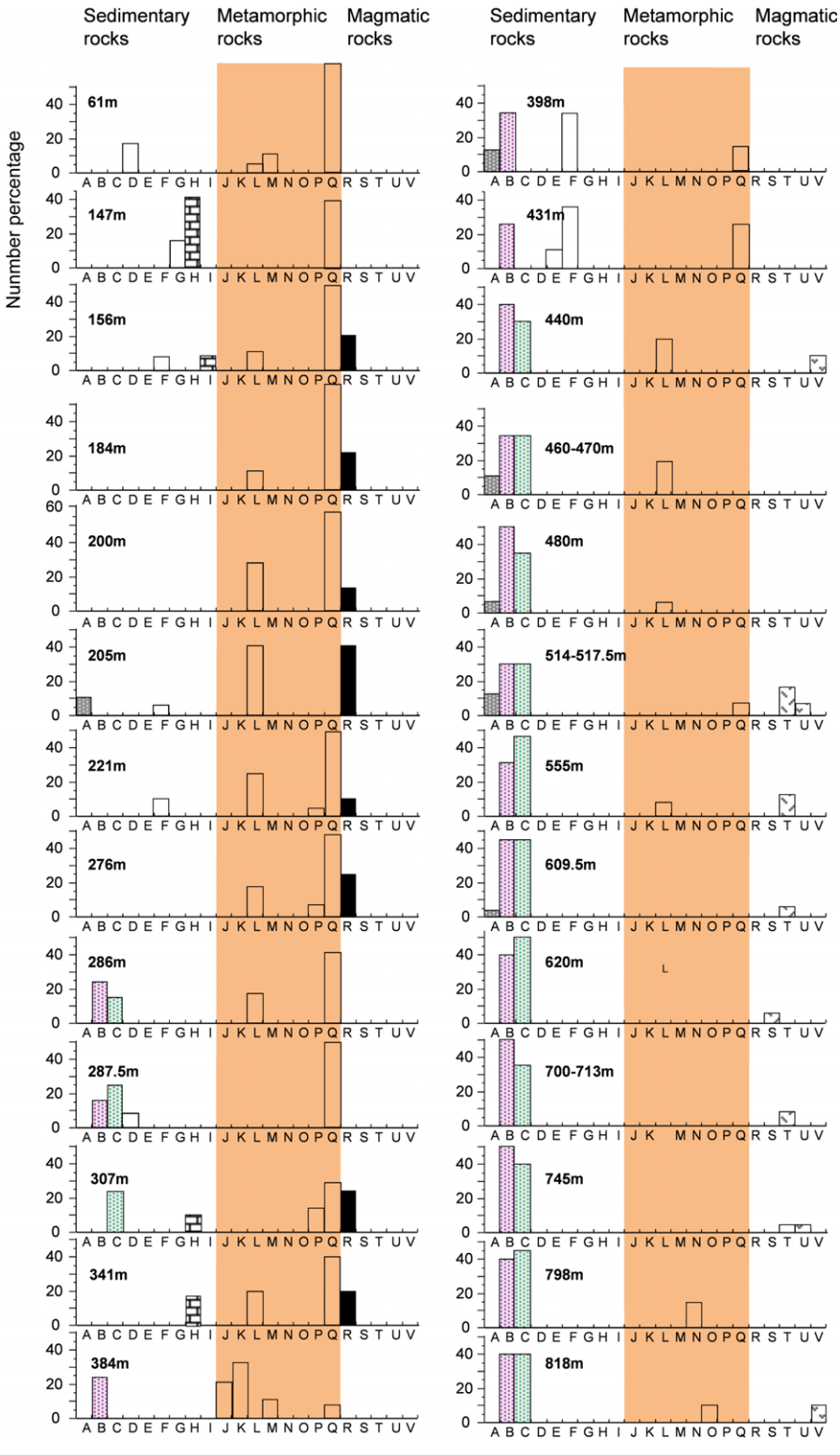

oblique- (cross-)bedded. The siltstones and mudstones are mostly massive with rare weak, horizontal laminations. We interpreted these features as channel and overbank deposits of moderately meandering rivers (Reading 1978; Fig. 13c).

The middle unit of the Shulehe Formation (383–823 m) consists of an alternating grey conglomerates–sandstones and yellowish brown siltstones–mudstones (Figs 12 & 13c). The conglomerates occur in large lenses and have imbricate structure, parallel and trough cross-beddings. The sandstones also occur in large lenses and have massive, parallel and occasionally cross-beddings. The siltstones and mudstones are generally massive. We interpreted these as braided river deposits (Reading 1978; Fig. 13c).

The third unit (823–916 m) consists predominantly of thick grey conglomerate layers, intercalated with thin brownish yellow sandstone and siltstone lens (Figs 12 & 13c). The conglomerates occur as thick layers and develop massive bedding with some boulders and weakly imbricate structure. We regarded these as debris flow and alluvial fan deposits (Reading 1978; Fig. 13c).

Variation of the sedimentation rate in the Sunan section lends support to the facies interpretation above (Fig. 13c, f). The sedimentation rate during deposition of the Baiyanghe Formation was the slowest (average 87.1 m/Ma) in the Sunan section (Fig. 13f). It matches the interpretation of a flood plain–playa depositional system with a deficiency of detrital supply (Reading 1978). The lower, middle and upper units of the Shulehe Formation have average sedimentation rates of about 111, 157 and 250 m/Ma, respectively (Fig. 13f). They agree well with the interpreted corresponding facies of a moderately meanding or braided river and alluvial fan (Fig. 13c) that require an increasing supply of detrital sediments (Reading 1978).

### *The Upper Yumu Shan section*

The Plio-Pleistocene conglomerate sequence in the Upper Yumu Shan section comprises conglomerate beds with a few small sandstone and siltstone lenses. These conglomerates develop weakly imbricate or massive structures, with many boulders. They are interpreted as debris flows and alluvial fan deposits (Reading 1978; Fig. 13c).

The gravel composition and palaeocurrent data provide information on mountain uplift and erosion. The main components of the gravels along the Sunan section are purple, green and yellow sandstones, granite and metamorphic rocks of quartzite and gneiss, with minor components of marl, mudstone, conglomerate, schist, mylonite, granulite, basalt and andesite in some beds (Fig. 12). Three distinct changes in gravel composition were found in the Sunan section. The measurements refer to heights within the measured section. Granite appears only in the rocks below the height 341–384 m (equivalent to *c*. 13 Ma), distinct purple, green and yellow sandstones generally occur above 276–286 m (*c*. 13.5 Ma), and metamorphic rocks decrease upwards and do not occur above the 559–609.5 m layer (*c*. 11.5–12 Ma; Fig. 12).

Palaeocurrent directions in the Sunan section trend weakly northward in the Baiyanghe Formation, persist northward in the Lower and Middle Shulehe Formation, and are stable southward from thickness 820 m (*c*. 9.8 Ma) in the Upper Shulehe direction (Fig. 13e). Stable northward palaeocurrents were also observed for the Upper Yumu Shan section (Fig. 13e).

## Discussion

### *Tectonic events and deformation: uplift history*

Based on the magnetostratigraphy and field tectonosedimentary investigations outlined above, we suggest that the North Qilian Shan and its associated Jiuquan foreland basin began to form from the Oligocene at the latest and the Yumu Shan uplift started in the late Miocene owing to a basinward transfer of deformation by propagation faults. This deformation and uplift are recorded as eight episodic tectonic events (Figs 13 & 14).

The occurrence of unconformity U1 at the base of the Sunan section and the deposition of the Beiyanghe Formation with dominantly northward current and gravels dominated by granite, gneiss and quartzite (Figs 5, 10 & 13) indicate that the eastern Jiuquan Basin began to subside and receive sediments from the North Qilian Shan beginning no later than 27.8 Ma in the Oligocene (Fig. 12a). The gravels of metamorphic rocks of gneiss and quartzite are typical components of Proterozoic rocks dominating Central Qilian Shan and southern part of the North Qilian Shan and do not appear in the Yumu Shan (Fig. 1a), suggesting an early uplift

**Fig. 12.** Variation of the gravel composition in the Sunan section. Gravel composition is expressed as a number percentage of an identified gravel to total counting gravels within an area of 1 × 1 m in the section. (**a**) Conglomerate; (**b**) purple sandstone; (**c**) greensandstone; (**d**) yellow sandstone; (**e**) grey sandstone; (**f**) other sandstones; (**g**) green-blue mudstones; (**h**) marl; (**i**) limestone; (**j**) leptynite; (**k**) schist; (**l**) gneiss; (**m**) jasper rock; (**n**) phyllonite; (**o**) chlorite schist; (**p**) mylonite; (**q**) siliceous rocks; (**r**) granite; (**s**) granodiorite; (**t**) diorite; (**u**) andesite; U, basalt.

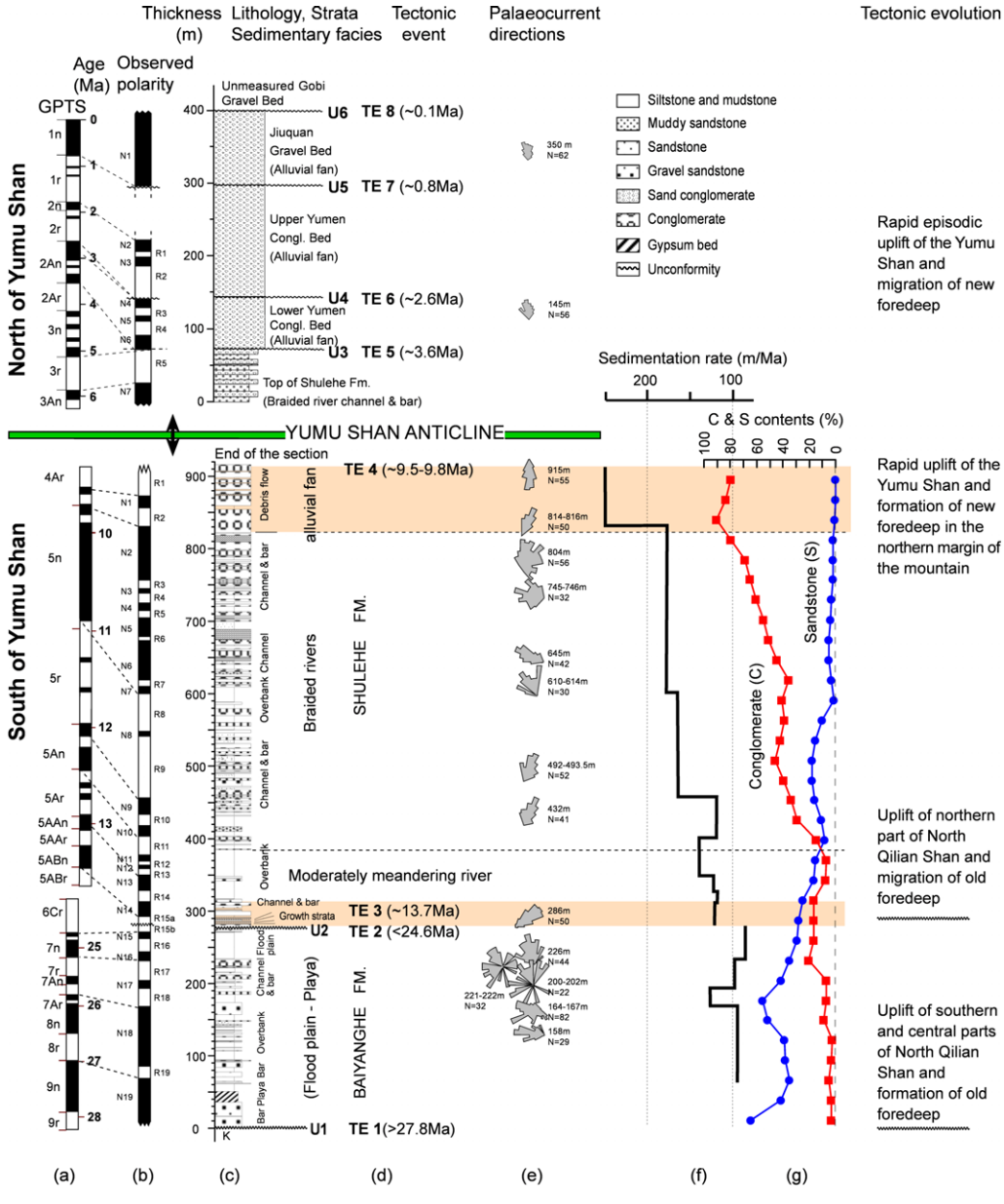


**Fig. 13.** Tectonosedimentary evolution of the Sunan and Upper Yumu Shan sections. River palaeocurrent directions (**e**) were obtained by statistical measurements of directions of gravel ab-faces. Sedimentation rate (**f**) was based on interpretation of magnetostratigraphy of the Sunan section in Figure 8. Percentage conglomerate and sandstone (**g**) were calculated from each 100 m stratigraphic interval using 25 m moving-window increments based on category of three statistic units: conglomerate, sandstone and siltstone–mudstone. This means that the rest is the percentage of siltstone–mudstone in the section, which is not present in the diagram.

and erosion of the North Qilian Shan. The fine sediments, playa–floodplain sedimentary environments, the weakly north-trending currents and the low sedimentation rate (average 87.1 m/Ma) during deposition of the Baiyanghe Formation in the Sunan section (Fig. 13) indicate slow subsidence of the Jiuquan Basin, a lowland with broad flat surface in the basin, and a deficiency of detrital supply

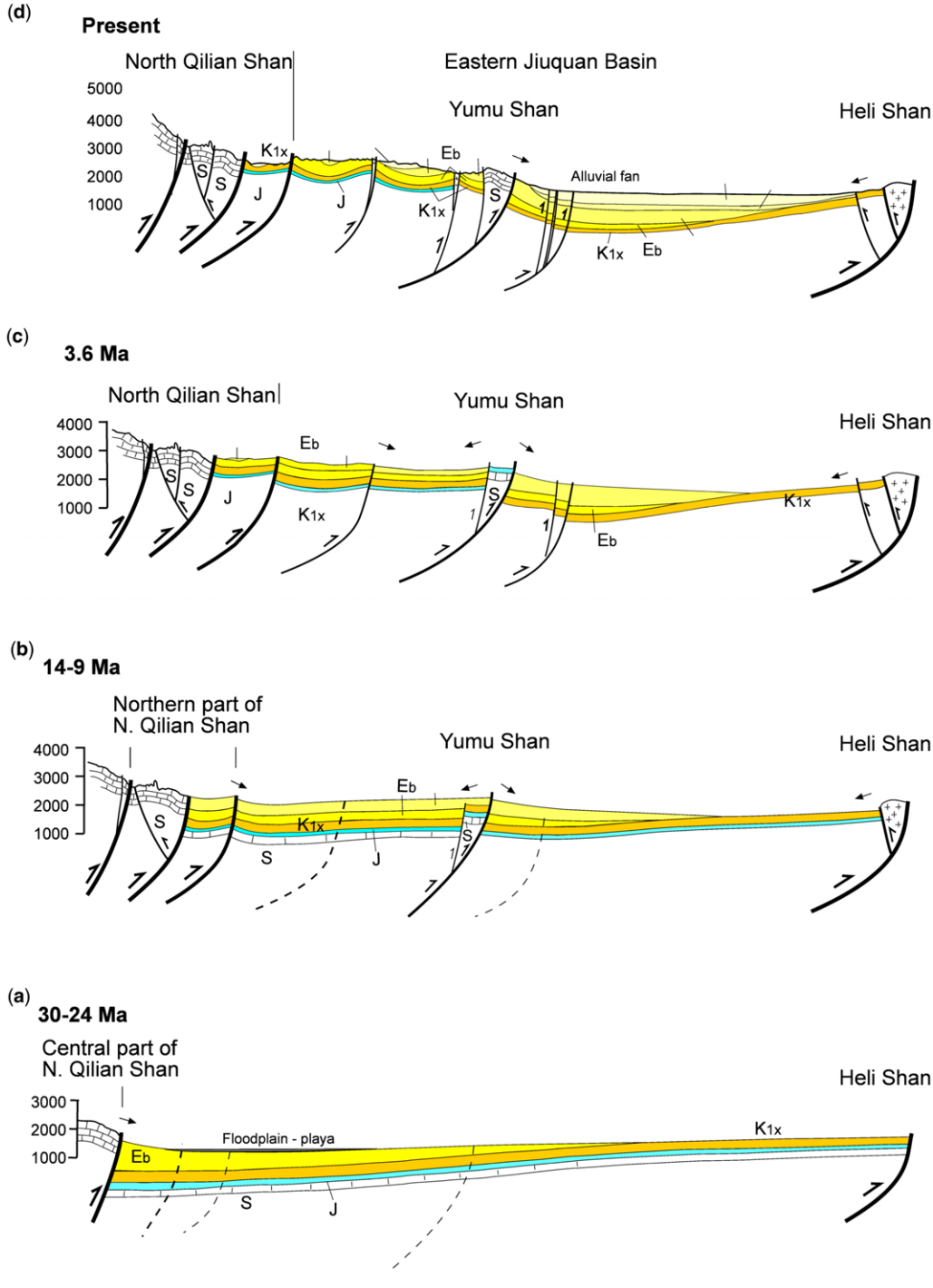


**Fig. 14.** Schematic diagram showing the Cenozoic uplift of the North Qilian Shan (NQS) and Yumu Shan and formation of the eastern Jiuquan foreland basin. Note the progressive northward migration of the foredeep and wedge-top of the Jiuquan foreland basin through progradation faults as responses in turn to uplifts of southern and central NQS, northern NQS and Yumu Shan. Marks for stratigraphic units and faults are same as those in Figure 1.

in the source area. By facies association, there must be coeval alluvial fan and braided river deposits further south in the Sunan section during deposition of the Baiyanghe Formation In fact, the Baiyanghe Formation is distributed in the northern part of the North Qilian Shan about 15–20 km south of the Sunan section, or further south in the western North Qilian Shan (Figs 1 & 3). Sedimentary facies and basin analyses revealed that these sediments do not reflect intermontane basin deposition but are connected with those in the Jiuquan Basin (Gansu Geologic Bureau 1989; EGPGYO 1989).

These data collectively suggest slow uplift of the southern and central parts of the North Qilian Shan (Fig. 13a). Southward thickening of the Baiyanghe Formation interpreted from a PetroChina borehole and seismostratigraphy (Fig. 1) suggests a flexural origin for the basin. The collision of India with Asia probably caused the rapid movement of Altun slip fault in Oligocene times (Yin *et al.* 2002) with subsequent compression and uplift from the North Qilian Shan (EGPGYO 1989) (Fig. 14a).

Deposition of the Baiyanghe Formation terminated at about 24.63 Ma, followed by a big gap in the unconformity U2 (24.63–13.7 Ma; Figs 10 & 13a–c). This suggests a second deformation and uplift of the basin and the Qilian Shan, most likely just at the end of the Baiyanghe Formation, because this unconformity is widely distributed in the Jiuquan Basin, and in the western Jiuquan Basin, the Shulehe Formation above the U2 is much thicker and has lower successions not occurring in the Sunan section. Its base age was estimated at the early Miocene by extrapolation of palaeomagnetically dated upper part of the Shulehe Formation (Fang *et al.* 2005*b*). This can be confirmed in the northern part of the eastern Jiuquan Basin just to the north of the Yumu Shan, where borehole and seismostratigraphy show that very thick Shulehe Formation (over twice as thick as that in the Sunan section and over three times thicker than the underlying Baiyanghe Formation) was deposited in the basin (Fig. 1c), suggesting a strong persistent flexing and subsiding of the Jiuquan Basin beginning in the early Miocene. We argue that this broad area of strong deformation of the Jiuquan Basin was caused by the intense uplift of the Qilian Shan probably in response to the growth of the Himalayas in the early Miocene (Yin & Harrison 2000; Tapponnier *et al.* 2001).

The bottom of the Shulehe Formation above the U2 unconformity starts with clear growth strata that occurred at about 13.7–13 Ma, accompanied by an increase of sedimentation rate over 115–150 m/Ma, a substantial conglomerate deposition, the first and important appearance of characteristic gravels of purple, green and yellow sandstones and the end or marked reduction of gravels of granite and metamorphic rocks, clear northward currents and a change in sedimentary environment from the previous playa–floodplain to a braided river (Figs 5 & 13). These observations collectively suggest another intense tectonic deformation of the basin through progradational faults and uplift of the northern part of the North Qilian Shan at latest at about 13.7–13 Ma (Fig. 14b), because the northern part of the North Qilian Shan consists of only Palaeozoic and Mesozoic rocks containing the characteristic gravels of purple, green and yellow sandstones (mostly from stratigraphy S, $J_3$ and $K_1$; Figs 1 & 3). In comparison with the much thicker Shulehe Formation in the northern part of the eastern Jiuquan Basin to the north of the Yumu Shan (Fig. 1c), we infer that the lower successions of the Shulehe Formation in the Sunan section were eroded away in this tectonic event. This site was probably subjected to rapid upheaval caused by the propagation fault. The subsequent deposition of sedimentary rocks with growth strata indicates a continuous but slow uplift of this site by the propagation fault. Taking into account that these sedimentary rocks in this rising site have a much higher sedimentation rate than previously deposited rocks (Fig. 13f ) and much thicker equivalent stratigraphy of the Shulehe Formation in the north of the Yumu Shan (Fig. 1c), we argue that the sedimentation rate increase in this site could not be related to the approach of the deformation front but must point to a much higher sedimentation rate increase and uplift from the North Qilian Shan.

From 820 m (*c.* 9.8 Ma), the former braided river system was replaced by debris flows and alluvial fan deposits, accompanied by a rapid increase in sedimentation rate (250 m/Ma), persistent occurrence of coarse conglomerates and change in former northward currents to stable southward currents. The Sunan section ends at 916 m (*c.* 9.6 Ma). All of this suggests that rapid uplift of the Yumu Shan, to the north of the Sunan section, began to occur at about 9.8–9.6 Ma, adding new sediments to the studied site (thus contributing to further increase of sedimentation rate), suggesting that the deformation was propagated into the inner basin through initiation of the NYF and its induced back-thrust fault (South Yumu Shan fault) from the North Qilian Shan (Figs 1, 3, 4 & 14b). Soon thereafter, the section was ended, suggesting that deformation and uplift of the North Qilian Shan and Yumu Shan accelerated, causing the studied site to be strongly faulted and folded. Thus, sedimentation in this region ceased and erosion commenced. This rise is about 8 million years earlier than the previous hypothesis that the Yumu Shan terrane was raised by the NYF at *c.* 1 Ma (see Fig. 15c in Meyer *et al.* 1998; Tapponnier *et al.* 1990, 2001). Rapid progradation of the NYF caused the previous (old) foredeep area to the

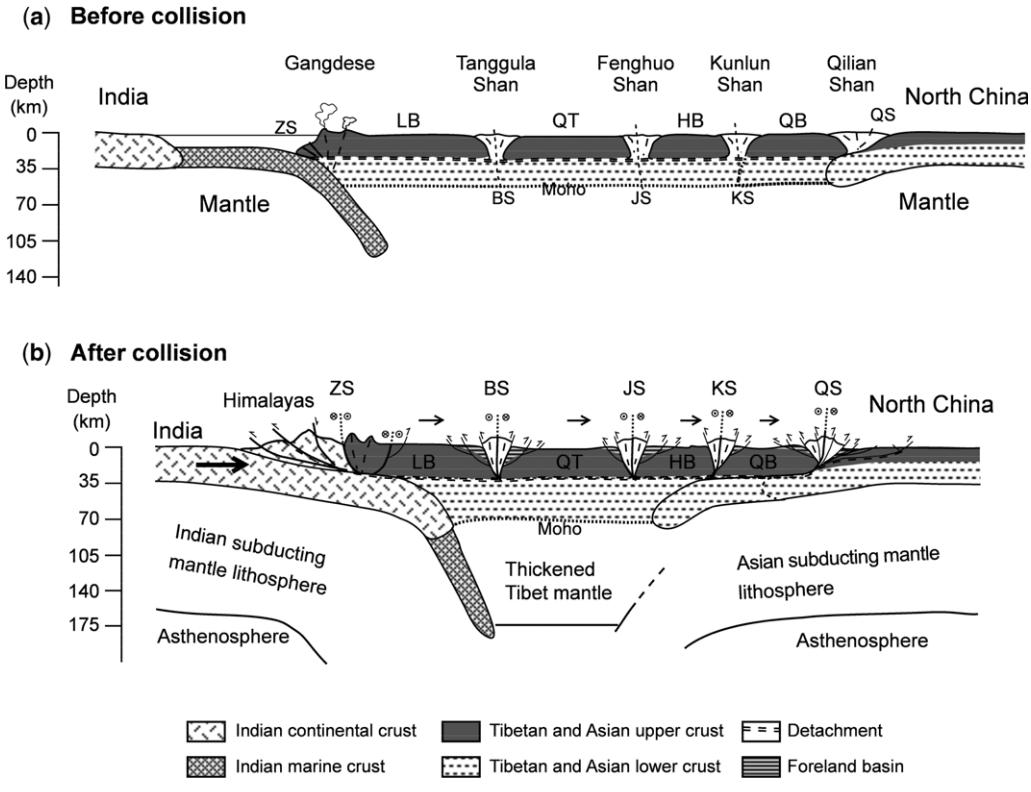


**Fig. 15.** Schematic diagram showing the process of rigid upper crust blocks detached from and floating on viscous lower crust and mantle of Tibet and synchronous differential deformation uplift of the Tibetan Plateau. Positions and boundaries of crusts, mantle lithospheres of India, Asia and Tibet (part of Asia) are referred to the literature (Tapponnier *et al.* 2001; Kind, *et al.* 2002; Kumar *et al.* 2006; Zhao *et al.* 2010). Arrows indicate moving direction and relative velocity. ZS, Zangbo suture; BS, Bangong suture; JS, Jinshan suture; KS, Kunlun suture; QS, Qilian suture; LB, Lhasa block; QB, Qiangtang block; HB, Hoxil block; QB, Qaidam block.

south of the Yumu Shan to be heaved up as wedge-top area (DeCelles *et al.* 1998) for erosion and new source rock supply and the previous slope area to the north of the Yumu Shan to be strongly flexed as a new foredeep area (Figs 1 & 14b).

The occurrences of the unconformities U3–U6 at about 3.6, 2.6, 0.8 and 0.1 Ma in the Upper Yumu Shan section (Figs 5, 10 & 13a–c), accompanied by persistent debris flow deposition, indicate the continuing episodic thrusting from the NYF and rapid uplifts of the Yumu Shan, resulting in very thick (over 2000 m) Plio-Quaternary sediments in the new foredeep (Fig. 14c, d).

### *Dynamic mechanism of deformation: uplift of NE Tibet: a proposed 'upper crust-floating model'*

The Oligocene deformation, uplift of the North Qilian Shan and flexing of the Hexi foreland basin revealed from detailed magnetostratigraphy and basin analysis are generally known from previous studies of the Kunlun–Qinling slip fault and Altun slip fault (e.g. Jolivet *et al.* 2001; Yin *et al.* 2002; Fang *et al.* 2003; Clark *et al.* 2010; Zhang *et al.* 2010) which may have been activated in the Eocene–Oligocene, and compression may have reached the North Qilian and east end of the Qilian Shan roughly at the same time (Fang *et al.* 2003; Dai *et al.* 2005). This challenges the current working models that are based either on the viscous or rigid lithosphere assumption. Both of these models regard the NE Tibetan Plateau, especially the northernmost part, the North Qilian Shan, as the final phase (Plio-Quaternary) of deformation and uplift of Tibet (Tapponnier *et al.* 1990, 2001; Meyer *et al.* 1998; England & Houseman 1988, 1989; Molnar *et al.* 1993; Royden *et al.* 1997, 2008).

The roughly synchronous (Eocene–Oligocene) response of deformation of the furthest north edge of the Tibetan Plateau to the main collision of

India with Asia at *c.* 50–40 Ma (Molnar & Tapponnier 1975; Patriat & Achache 1984; Rowley 1996) suggests that the collision stress reached the northern edge of the Tibetan Plateau rapidly. This requires the block to have a rigid nature. Mechanically, for a vast block like Tibet, *c.* 3500 × 1500 km (*c.* 2 500 000 $km^2$; Fielding *et al.* 1994), if its whole lithosphere acts as a rigid block, it is impossible to pass push-stress from the southern edge to the northern one; instead it will break the block immediately north of the push zone (or along some nearby weak zone like a former suture, as indicated by Tapponnier *et al.* 2001), owing to the great resistance of the rigid block. Further push will accumulate stress and migrate northward to make a new break. This process will follow the pathway to cause a stepwise rise and growth of Tibet, such as that proposed by Tapponnier's group (Tapponnier *et al.* 1990, 2001; Meyer *et al.* 1998).

In such a large rigid block (upper crust) floating on a viscous lower crust with a detachment, a push from the southern edge of a rigid block will easily and immediately pass on to the northern edge, just like pushing on a large wood board floating on water. Since the Tibetan Plateau consists of several Tethys blocks separated by narrow ranges and sutures (Fig. 1 inset), we regard the Tibet upper crust as rigid blocks separated by narrow 'soft' ranges and sutures, and assume that these 'range-conjuncted' upper crust blocks were detached to a considerable extent (if not entirely) and floated on their viscous lower crusts and mantles at each collision of the Tethys blocks with Palaeo-Asia before the India–Asia collision. Thus, when India collided with Asia, the Tibet upper crust would rapidly float northwards, passing compressive stress and deformation northwards immediately into inner and NE Tibet through rigid blocks, activating former sutures and deep faults, uplifting inter-block ranges and forming new thrust–fold systems, probably connecting with former (or new) detachments and foreland basins along margins of ranges, while the Tibet lower crust and mantle would be subjected to continuous thickening differentially from both the southern and northern sides (larger in the south and smaller in the north), thus probably also creeping northwards, because the southern and northern margins of Tibet experience positive and passive underthrusting and compression, respectively, and the buffering (thus attenuated deformation in magnitude) of 'soft ranges' between rigid blocks (Fig. 15b). In consequence, the Altun fault would have formed shortly after the India–Asia collision initially at *c.* 55 Ma and mainly at *c.* 50–40 Ma (Molnar & Tapponnier 1975; Patriat & Achache 1984; Rowley 1996), and the former sutures and deep faults bounding the Qilian Shan (Molnar & Tapponnier 1975; Gansu Geologic Bureau 1989; Feng & Wu 1992) would have been activated coevally and detached from the North China lower crust and mantle as the latter passively moved southwards and plunged beneath the Kunlun Shan, causing synchronous Eocene–Oligocene deformation, uplift of the Qilian Shan and formation of flexural foreland basins along its rims (Fig. 15b). When there was no further accommodation for deformation of 'soft ranges' south of the Qilian Shan, compressive stress would have transferred to the NE edge, leading to a later-phase (Miocene–Quaternary) of rapid deformation and uplift of the North Qilian Shan and Yumu Shan (Fig. 15b).

A complete discussion and summary of evidence to support this model is beyond the scope of the paper. Here we outline evidence which supports the model.

Theoretical calculation and modelling have shown that the lower crust may act as a viscous thin layer that might flow out mostly southwards, northwards and eastwards along channels (Royden 1996; Royden *et al.* 1997, 2008). Exposed leucogranites and the metamorphic sequence in the Himalayas have been recognized to indicate lower crust partial melting and channel flow (Le Fort *et al.* 1987; Yin & Harrison 2000; Beaumont *et al.* 2001; Grujic *et al.* 2002).

Recent magnetotelluric data confirm that such a channel flow existed along at least 1000 km of the southern margin of the Tibetan plateau (Unsworth *et al.* 2005), and also in a vast area from central-east Tibet to SW China at a depth of 20–40 km (Bai *et al.* 2010). This is concordant with the notion that a lower-velocity (thus weaker) zone of P-wave in middle–lower crust is commonly observed beneath Tibet (Kind *et al.* 2002; Kumar *et al.* 2006; Zhao *et al.* 2010). Seismic tomography clearly shows the existence of detachment surfaces between upper and middle–lower crusts beneath the Qilian Shan, Kunlun Shan and other ranges of Tibet and Himalayas (Gao *et al.* 1995; Tapponnier *et al.* 2001; Kumar *et al.* 2006; Zhao *et al.* 2010).

Recent recognition and dating of the slip-related and flexural-depressed basins along the margins of ranges on the Tibetan Plateau demonstrate that they formed at roughly the same time, at *c.* 50–40 Ma (e.g. Decelles *et al.* 1998; Horton *et al.* 2002; Fang *et al.* 2003; Dai *et al.* 2005; Wang *et al.* 2008), corroborating the Eocene rapid rise and exhumation events detected in related ranges from the south to the NE Tibetan Plateau by a variety of thermochronology methods (Jolivet *et al.* 2001; Wang *et al.* 2008; Clark *et al.* 2010).

Modern GPS observation indicates clearly that the whole Tibetan Plateau is primarily under simultaneous but differential shortening in a north–south direction, with the shortening rate decreasing from *c.* 15–20 mm $a^{-1}$ in the Himalayas, through

*c*. 12–9 mm $a^{-1}$ in the central and north Tibet, to *c*. 6 mm $a^{-1}$ in northeastern Tibet (Zhang *et al.* 2004). This provides a robust support for our model that Tibetan rigid upper crust blocks buffered by inter-block soft ranges and sutures float and move northeastwards on a viscous lower crust (Fig. 15).

## Conclusions

(1) High-resolution magnetostratigraphy constrains the age range of the Sunan section between the North Qilian Shan and the Yumu Shan at about 27.8–9.6 Ma, and the Upper Yumu Shan section to the north of the Yumu Shan at about 6.1 and 0.1 Ma, with stratigraphic units of the Baiyanghe Formation at about 27.8–24.63 Ma, the Shulehe Formation at about 13.69–3.6 Ma, and the Yumen, Jiuquan and Gobi Conglomerate (Gravel) Beds at about 3.6–0.9, 0.8–0.1 and 0.1 Ma, respectively.

(2) Tectonosedimentological studies and basin analysis suggest that eight tectonic events occurred at about 27.8, 24.6, 13.7, 9.8–9.5, 3.6, 2.6, 0.8 and 0.1 Ma, recording an early (Oligocene) slow and later (Miocene–Quaternary) episodic rapid uplift of the North Qilian Shan and formation of the Jiuquan foreland basin. The Yumu Shan at the northeasternmost corner of the Qilian Shan began to uplift rapidly at latest at about 9.8–9.6 Ma, rather than the previously thought much later (*c*. 1 Ma) rise, thus challenging the commonly accepted tectonic model of the oblique stepwise rise of the Tibetan Plateau and northeastward growth of the Qilian Shan and Yumu Shan (Tapponnier *et al.* 1990, 2001). Rigid blocks floating on viscous lower crust, called the 'block-floating model', is proposed to interpret this early and episodic response to Indian–Asian collision.

This work was supported by National Natural Science Foundation of China grants (41021001, 40920114001) and the (973) National Basic Research Program of China (grant no. 2011CB403000). We thank L.L.X. Zhang, W. Ma, Y. Tang, Y. Liu, Q. Xu, S. Hu and Z. Zhang for field-work assistance. We also thank Y. Liu, J. Wang and Y. Chen for laboratory help. Special thanks are due to Professor R. Zhu for his continual laboratory support, Professors Z. Junmeng and H. Jiankun for their constructive discussions, Professor Y. An for critical comments on an earlier version of the manuscript, and Yumen Oil Field Com., PetroChina for providing and permitting use of their seismic data. We finally thank Professor R. Burmester and an anonymous reviewer for their constructive comments which helped to improve the manuscript greatly.

## References

Bai, D. H., Unsworth, M. J. *et al.* 2010. Crustal deformation of the eastern Tibetan plateau revealed by magnetotelluric imaging. *Nature Geosciences*, http://dx.doi.org/10.1038/NGEO830

Beaumont, C., Jamieson, R. A., Nguyen, M. H. & Lee, B. 2001. Himalayan tectonics explained by extrusion of a low-viscosity crustal channel coupled to focused surface denudation. *Nature*, **414**, 738–742.

Burchfiel, B. C., Deng, Q. *et al.* 1989. Intracrustal detachment within zones of continental deformation. *Geology*, **17**, 448–452.

Cande, S. C. & Kent, D. V. 1995. Revised calibration of the geomagnetic polarity timescale for the late Cretaceous and Cenozoic. *Journal of Geophysical Research*, **100**, 6093–6095.

Charreau, J., Chen, Y. *et al.* 2009. Neogene uplift of theTian Shan Mountains observed in the magnetic record of the Jingou River section (northwest China). *Tectonics*, **28**, http://dx.doi.org/10.1029/2007TC002137

Chung, S. L., Lo, C. C. *et al.* 1998. Diachronous uplift of the Tibetan plateau starting 40 Myr ago. *Nature*, **394**, 769–73.

Clark, M. K., Farley, K. A., Zheng, D. W., Wang, Z. C. & Duvall, A. R. 2010. Early Cenozoic faulting of the northern Tibetan Plateau margin from apatite (U–Th)/He ages. *Earth and Planetary Science Letters*, **296**, 78–88.

Coleman, M. E. & Hodges, K. V. 1995. Evidence for Tibetan Plateau uplift before 14 Myr ago from a new minimum estimate for east–west extension. *Nature*, **374**, 49–52.

Dai, S. A., Fang, X. M., Song, C. H., Gao, J. P., Gao, D. L. & Li, J. J. 2005. Early tectonic uplift of the northern Tibetan Plateau. *Chinese Science Bulletin*, **50**, 1642–1652.

Decelles, P. G., Gehrels, G. E., Quade, J. & Ojha, T. P. 1998. Eocene–early Miocene foreland basin development and the histroy of Himalayas thrusting, western and central Nepal. *Tectonics*, **17**, 741–765.

Dewey, J. F., Shackleton, R. M., Chang, C. & Yiyin, S. 1988. The tectonic evolution of the Tibetan Plateau. *Philosophical Transactions of the Royal Society of London, A*, **327**, 379–413.

EGPGYO (EDITORAL GROUP OF PETROLEUM GEOLOGY OF YUMEN OILFIELD), 1989. *Petroleum Geology of China. Yumen Oilfield*, Vol. **13**. Petroleum Industry Publishing, Beijing, 1–441.

England, P. C. & Houseman, G. A. 1986. Finite strain calculations of continental deformation, 2. *comparison with the India–Asia collision zone*. *Journal of Geophysical Research*, **91**, 3664–3676.

England, P. C. & Houseman, G. A. 1988. The mechanics of the Tibetan Plateau [and discussion]. *Philosophical Transactions of the Royal Society of London A*, **326**, 301–320.

England, P. C. & Houseman, G. A. 1989. Extension during continental convergence, with application to the Tibetan Plateau. *Journal of Geophysical Research*, **94**, 17 561–17 579.

Fang, X. M., Garzione, C., Van Der Voo, R., Li, J. J. & Fan, M. J. 2003. Flexural subsidence by 29 Ma on the

NE edge of Tibet from the magnetostratigraphy of Linxia Basin, China. *Earth and Planetary Science Letters*, **210**, 545–560.

FANG, X. M., YAN, M. D. *ET AL.* 2005*a*. Late Cenozoic deformation and uplift of the NE Tibetan plateau: evidence from high-resolution magneto stratigraphy of the Guide Basin, Qinghai Province, China. *GSA Bulletin*, **117**, 1208–1225.

FANG, X. M., ZHAO, Z. J. *ET AL.* 2005*b*. Magnetostratigraphy of the late Cenozoic Laojunmiao anticline in the northern Qilian Mountains and its implications for the northern Tibetan Plateau uplift. *Science in China Series D: Earth Science*, **48**, 1040–1051.

FENG, Y. M. & WU, H. Q. 1992. Tectonic evolution of North Qilian Mountains and its neighbourhood since Paleozoic. *Northwest Geoscience*, **13**, 61–74 (in Chinese with English abstract).

FIELDING, E., ISACKS, B., BARAZANGI, M. & DUNCAN, C. C. 1994. How flat is Tibet? *Geology*, **22**, 163–167.

GANSU GEOLOGIC BUREAU. 1971. *Geologic Map of Sunan, 1:200 000 (with Guide Book)*. Gansu Publishing House, Lanzhou (in Chinese).

GANSU GEOLOGIC BUREAU. 1989. *Regional Geology Evolution of Gansu Province*. Geological Publishing House, Beijing (in Chinese).

GAO, R., CHENG, X. Z. & DING, Q. 1995. Preliminary geodynamic model of Golmud-Ejin Qi geoscience transect. *Journal of Geophysics*, **38**(suppl. I), 3–14 (in Chinese with English abstract).

GARCÉS, M., AGUST, I. J., CABRERA, L. & PAÉS, J. M. 1996. Magnetostratigraphy of the Vallesian (late Miocene) in the Vallès-Penedès basin (NE Spain). *Earth and Planetary Science Letters*, **142**, 381–396.

GEORGE, A. D., MARSHALLSEA, S. J., WYRWOLL, K. H., CHEN, J. & LU, Y. C. 2001. Miocene cooling in the Northern Qilian Shan, northeastern margin of the Tibetan Plateau, revealed by apatite fission-track and vitrinite reflectance analysis. *Geology*, **29**, 939–942.

GRUJIC, D., HOLLISTER, L. S. & PARRISH, R. R. 2002. Himalayan metamorphic sequence as an orogenic channel: insight from Bhutan. *Earth and Planetary Science Letters*, **198**, 177–191.

HARRISION, T. M., COPELAND, P., KIDD, W. S. F. & YIN, A. 1992. Raising Tibet. *Science*, **255**, 1663–1670.

HE, G. Y., YANG, S. F., CHEN, H. L., XIAO, A. C. & CHENG, X. G. 2004. New ideas about the Early Cretaceous basins in western Gansu Corridor and nearby regions. *Acta Petrologica Sinica*, **25**, 18–22 (in Chinese with English Abstract).

HORTON, B. K., YIN, A., SPURLIN, M. S., ZHOU, J. & WANG, J. 2002. Paleocene–Eocene syncontractional sedimentation in narrow, lacustrine-dominated basins of east-central Tibet. *Geologic Society of American Bulletin*, **114**, 771–786.

HUANG, H. F., PENG, Z. L., LU, W. & ZHENG, J. J. 1993. Paleomagnetic division and comparison of the tertiary system in Jiuxi and Jiudong basins. *Acta Geologica Gansu*, **2**, 6–16 (in Chinese with English Abstract).

JOLIVET, M., BRUNEL, M. *ET AL.* 2001. Mesozoic and Cenozoic tectonics of the northern edge of the Tibetan plateau: fission-track constraints. *Tectonophysics*, **343**, 111–134.

KIND, R., YUAN, X. *ET AL.* 2002. Seismic images of crust and upper mantle beneath Tibet: evidence for Eurasian plate subduction. *Science*, **298**, 1219–1221.

KUMAR, P., YUAN, X., KIND, R. & NI, J. (2006) Imaging the colliding Indian and Asian lithospheric plates beneath Tibet. *Journal of Geophysical Research*, **111**, http://dx.doi.org/10.1029/2005JB003930

LE FORT, P., CUNEY, M. *ET AL.* 1987. Crustal generation of the Himalayan leucogranites. *Tectonophysics*, **134**, 39–57.

LI, J. J., FANG, X. M. *ET AL.* 1997. Late Cenozoic magnetostratigraphy (11–0 Ma) of the Dongshanding and Wangjiashan sections in the Longzhong Basin, western China. *Geologie en Mijnbouw*, **76**, 121–134.

LIU, D. L., FANG, X. M. *ET AL.* 2010. Stratigraphic and paleomagnetic evidence of mid-Pleistocene rapid deformation and uplift of the NE Tibetan Plateau. *Tectonophysics*, **486**, 108–119.

MCELHINNY, M. W. 1964. Statistical significance of the Fold Test in paleomagnetism. *Geophysical Journal of the Royal Astronomical Society*, **8**, 33–40.

METIVER, F., GAUDEMER, Y., TAPPONNIER, P. & MEYER, B. 1998. Northeastward growth of the Tibet plateau deduced from balanced reconstruction of two depositional areas: the Qaidam and Hexi Corridor basins, China. *Tectonics*, **17**, 823–842.

MEYER, B., TAPPONNIER, P. *ET AL.* 1998. Crustal thickening in Gansu–Qinghai, lithospheric mantle subduction, and oblique, strike-slip controlled growth of the Tibet plateau. *Geophysics Journal International*, **135**, 1–47.

MOLNAR, P. & TAPPONNIER, P. 1975. Cenozoic tectonics of Asia – effects of a continental collision. *Science*, **189**, 419–426.

MOLNAR, P., ENGLAND, P. C. & MARTINOD, J. 1993. Mantle dynamics, uplift of the Tibetan Plateau, and the Indian Monsoon. *Review of Geophysics*, **31**, 357–396.

NI, J. & BARAZANGI, M. 1984. Seismotectonics of the Himalayan collision zone: geometry of the underthrusting Indian Plate beneath the Himalaya. *Journal of Geophysical Research*, **89**, 1147–1163.

PATRIAT, P. & ACHACHE, J. 1984. India–Eurasia collision chronology has implications for crustal shortening and driving mechanism of plates. *Nature*, **311**, 615–621.

READING, H. G. 1978. *Sedimentary Environments and Facies*. Blackwell Science, Oxford, 1–557.

ROWLEY, D. B. 1996. Age of initiation of collision between Indian and Asia: a review of stratigraphic data. *Earth and Planetary Science Letters*, **145**, 1–13.

ROYDEN, L. H. 1996. Coupling and decoupling of crust and mantle in convergent orogens: implications for strain partitioning in the crust. *Journal of Geophysical Research*, **101**, 17 679–17 705.

ROYDEN, L. H., BURCHFIEL, B. C. *ET AL.* 1997. Surface deformation and lower crustal flow in eastern Tibet. *Science*, **276**, 788–790.

ROYDEN, L. H., BURCHFIEL, B. C. & VAN DER HILST, R. D. 2008. The geological evolution of the Tibetan Plateau. *Science*, **321**, 1054–1058.

TAPPONNIER, P., MEYER, B. *ET AL.* 1990. Active thrusting and folding in the Qilian Shan, and decoupling between upper crust and mantle in northeastern Tibet. *Earth and Planetary Science Letters*, **97**, 382–403.

TAPPONNIER, P., XU, Z. Q. *ET AL.* 2001. Geology – oblique stepwise rise and growth of the Tibet plateau. *Science*, **294**, 1671–1677.

TAUXE, L. & GALLET, Y. 1991. A jackknife for magnetostratigraphy. *Geophysical Research Letters*, **18**, 1783–1786.

TAUXE, L. 1998. *Paleomagnetic Principles and Practice*. Kluwer Academic, Dordrecht, 121–170.

TURNER, S., HAWKESWORTH, C., LIU, J., ROGERS, N., KELLEY, S. & VAN CALSTEREN, P. 1993. Timing of Tibetan uplift constrained by analysis of volcanic rocks. *Nature*, **364**, 50–54.

UNSWORTH, M. J., JONES, A. G., WEI, W., MARQUIS, G., GOKARN, S. G., SPRATT, J. E. & THE INDEPTH-MT TEAM 2005. Crustal rheology of the Himalaya and Southern Tibet inferred from magnetotelluric data. *Nature*, **438**, 78–81.

WANG, S. 1965. Cenozoic stoneworts in the Jiuquan Basin, Gansu. *Acta Petrologica Sinica*, **13**, 463–509 (in Chinese with English abstract).

WANG, Q. M. & COWARD, M. P. 1993. The Jiuxi Basin, Hexi Corridor, NW China: Foreland structural features and hydrocarbon potential. *Journal of Petroleum Geology*, **16**, 169–182.

WANG, C. S. *ET AL.* 2008. Constraints on the early uplift history of the Tibetan Plateau. *Proceedings of the National Academy of Sciences USA*, **105**, 4987–4992.

YIN, A. & HARRISON, T. M. 2000. Geologic evolution of the Himalayan–Tibetan orogen. *Annual Review of Earth and Planetary Sciences*, **28**, 211–280.

YIN, A., RUMELHART, P. E. *ET AL.* 2002. Tectonic history of the Altyn Tagh fault system in northern Tibet inferred from Cenozoic sedimentation. *GSA Bulletin*, **114**, 1257–1295.

ZHANG, P. Z. *ET AL.* 2004. Continuous deformation of the Tibetan Plateau from global positioning system data. *Geology*, **32**, 809–812.

ZHANG, J., CUNNINGHAM, W. D. & CHENG, H. Y. 2010. Sedimentary characteristics of Cenozoic strata in central-southern Ningxia, NW China: Implications for the evolution of the NE Qinghai-Tibetan Plateau. *Journal of Asian Earth Sciences*, **39**, 740–759.

ZHAO, J. M. *ET AL.* 2010. The boundary between the Indian and Asian tectonic plates below Tibet. *Proceedings of the National Academy of Sciences USA*, **107**, 11 229–11 233.